RUNX1 mitotically bookmarks target genes that are important for the mammary epithelial-to-mesenchymal transition

Joshua T. Rose[1,§], Eliana Moskovitz[1,§], Joseph R. Boyd[1], Jonathan A. Gordon[1], Nicole A. Bouffard[2], Andrew J. Fritz[1], Anuradha Illendula[3], John H. Bushweller[3], Jane B. Lian[1], Janet L. Stein[1], Gary S. Stein[1], and Sayyed K. Zaidi[1#]

[1]Department of Biochemistry and University of Vermont Cancer Center, Robert Larner College of Medicine, 89 Beaumont Avenue, Burlington, VT 05405, USA

[2]Microscopy Imaging Center at the Robert Larner College of Medicine, 89 Beaumont Avenue, Burlington, VT 05405, USA

[3]Department of Molecular Physiology and Biological Physics, University of Virginia, Charlottesville, VA 22908, USA

[§]These authors contributed equally

[#]Corresponding Author

Sayyed K Zaidi, PhD

sayyed.zaidi@med.uvm.edu

Room E210, Given Building

University of Vermont

89 Beaumont Avenue, Burlington VT 05405

Key Words: Mammary phenotype, epithelial phenotype, RUNX1, mitotic gene bookmarking.

27 **Significance:**

28 This study elucidates mitotic gene bookmarking as a potential epigenetic
29 mechanism that impacts breast epithelial cell growth and phenotype and has potential
30 implications in breast cancer onset.

ABSTRACT

RUNX1 has recently been shown to play an important role in determination of mammary epithelial cell identity. However, mechanisms by which loss of the RUNX1 transcription factor in mammary epithelial cells leads to epithelial-to-mesenchymal transition (EMT) are not known. Here, we report mitotic bookmarking of genes by RUNX1 as a potential mechanism to convey regulatory information through successive cell divisions for coordinate control of mammary cell proliferation, growth, and identity. Genome-wide RUNX1 occupancy profiles for asynchronous, mitotically enriched, and early G1 breast epithelial cells reveal RUNX1 is retained during the mitosis to G1 transition on protein coding and long non-coding RNA genes critical for mammary epithelial proliferation, growth, and phenotype maintenance. Disruption of RUNX1 DNA binding and association with mitotic chromosomes alters cell morphology, global protein synthesis, and phenotype-related gene expression. Together, these findings show for the first time that RUNX1 bookmarks a subset of epithelial-related genes during mitosis that remain occupied as cells enter the next cell cycle. Compromising RUNX1 DNA binding initiates EMT, an essential first step in the onset of breast cancer.

INTRODUCTION

Breast cancer arises from a series of acquired mutations and epigenetic changes that disrupt normal mammary epithelial homeostasis and create multi-potent cells that can differentiate into biologically unique and clinically distinct subtypes (1-6). Epithelial-to-mesenchymal transition (EMT)—a trans-differentiation process through which mammary epithelial cells acquire the aggressive mesenchymal phenotype—is a key driver of breast cancer progression, invasion and metastasis (7-12). Transcription factors Snail, Slug, Twist, and Zeb1/2 contribute to EMT during early, normal development and have also been implicated in invasion (13-16). Despite accumulating evidence that defines a broad understanding of EMT regulation and maintenance of the epithelial phenotype (7-12), the mechanism(s) by which mammary cells maintain their epithelial phenotype is unknown.

Runt-Related Transcription Factor 1 (RUNX1/AML1) is required for hematopoietic lineage specification during development and hematopoiesis throughout life (17-30). In addition to the recognized role in hematological malignancies, RUNX1 has been recently identified as a key player in breast cancer development and tumor progression (31-38). Findings from our group (39), reinforced by studies from others (40, 41), have shown that RUNX1 plays a critical role in maintaining breast epithelial phenotype and prevents EMT through transcriptional regulation of genes (e.g., the EMT marker and a key cell adhesion protein E-cadherin) involved in fundamental cellular pathways. However, mechanisms by which RUNX1 prevents EMT have not been identified.

Mitotic gene bookmarking, i.e. transcription factor binding to target genes during mitosis for transcriptional regulation following cell division, is a key epigenetic mechanism

to convey and sustain regulatory information for cell proliferation, growth, and cell identity from parent to progeny cells (42-49). We have established that RUNX proteins, as well as other phenotypic transcription factors that include MYOD and CEBPα, mitotically bookmark RNA Pol I- and II-transcribed genes in osteoblasts and leukemia cells for coordinate control of cell growth, proliferation and phenotype (50-57). It is increasingly evident that mitotic gene bookmarking by transcription factors is a key mechanism to determine and maintain cell fate across successive cell divisions (58-70).

We addressed the hypothesis that RUNX1 maintains the breast epithelial phenotype by mitotic bookmarking of genes that support mammary epithelial proliferation, growth, and phenotype for expression in the next cell cycle. Fluorescence confocal microscopy of fixed and live mammary epithelial cells revealed that RUNX1 is present on chromosomes throughout mitosis and colocalizes with upstream binding transcription factor (UBF), a subunit of RNA Pol I transcriptional machinery (71). To identify genes occupied by RUNX1, we performed chromatin immunoprecipitation coupled with high throughput sequencing (ChIP-Seq) using a RUNX1-specific antibody on mitotic, G1, and asynchronous normal mammary epithelial MCF10A cells. As expected, ribosomal RNA genes, regulated by the RNA Pol I transcriptional machinery, were occupied by RUNX1. A fluorescence-based, global protein synthesis assay showed reduced protein synthesis when RUNX1 DNA binding was perturbed using a small molecule inhibitor. Importantly, ChIP-Seq revealed that, in mitosis, RUNX1 associates with RNA Pol II regulated genes specifically involved in maintenance of the epithelial phenotype and EMT progression. Strikingly, disruption of RUNX1 DNA binding, which is required for association with mitotic chromosomes (56), results in loss of the epithelial phenotype and acquisition of

mesenchymal properties that are accompanied by changes in expression of associated genes and pathways and represent early events in the onset of breast cancer. These findings implicate RUNX1 occupancy of target genes at the mitosis into G1 transition in regulating the normal breast epithelial phenotype.

RESULTS

RUNX1 associates with mitotic chromatin and occupies target genes

To investigate subcellular localization of RUNX1 in normal mammary epithelial cells, we performed immunofluorescence (IF) microscopy in actively proliferating MCF10A cells and imaged cells undergoing spontaneous mitoses. We observed that RUNX1 is localized on mitotic chromatin at all topologically identified substages of mitosis (Fig. 1; top panels). Two distinct types of foci are detectable on mitotic chromosomes: 2-8 large punctate foci that appear to be allelic as well as numerous smaller foci that are distributed across the chromosomes (Fig. 1; bottom panels, white arrowheads). In all replicates, important secondary-antibody-only controls were included to confirm specificity of RUNX1 signal on mitotic chromosomes (Suppl. Fig. 1). In the interphase nuclei, RUNX1 exhibited the characteristic punctate distribution (Fig. 1; interphase panel). To ensure reproducibility of our findings, the IF experiments were repeated at least 3 times and, at the minimum, 20 interphase and mitotic cells were imaged.

Multiple reports have indicated that formaldehyde fixation can prevent regulatory protein detection on mitotic chromosomes (58, 69). To further confirm that association of RUNX1 with mitotic chromosomes is not under-represented because of formaldehyde fixation, we examined the localization of RUNX1-EGFP in actively proliferating, unfixed MCF10A cells. Consistent with our findings in fixed and synchronized cells, RUNX1-EGFP was associated with chromosomes in live MCF10A cells undergoing mitosis (Suppl. Fig. 2.). Together, these findings establish that RUNX1 foci are present on chromosomes at all stages of mitosis under physiological conditions in actively dividing,

unfixed breast epithelial cells and, in agreement with our previous findings, are equally distributed into resulting progeny cells (57).

To experimentally address whether RUNX1 presence on mitotic chromosomes reflects occupancy of target genes, MCF10A cells were synchronized in mitosis using nocodazole (50ng/mL; Supp. Fig. 3A). Nocodazole dose and treatment were empirically determined to minimize toxic effects of the drug, while maximizing mitotic enrichment. Mitotic cells were collected by mitotic shake-off and purity of harvested cells was confirmed by the presence of H3pS28 in >70% of cells. We chose the H3pS28 mark to identify mitotic cells because this histone mark is highly specific to condensed chromosomes during mitosis; more commonly used H3pS10 mark is additionally observed in early G1 cells and has also been associated with replicating centers in S-phase (72, 73). A parallel, nocodazole-treated cell population was released into early G1 by replacing nocodazole-containing growth medium with fresh, nocodazole-free, growth medium and was harvested 3 hours post-release (Suppl. Fig. 3B). Western blot analysis of whole cell lysates from the three cell populations showed expected levels of expression for cell cycle-specific proteins Cyclin B and CDT1 (Suppl. Fig. 3C). FACS profiles of the cell populations confirmed the characteristic enrichment of blocked cells in mitosis (Supp. Fig. 3D; Mitotic) and release into G1 upon media replacement (Supp. Fig. 3D; G1) when compared to asynchronous cells (Supp. Fig. 3D; Asynch). To determine whether RUNX1 remains bound to target genes during mitosis, ChIP-Seq was performed on Asynch, Mitotic, and G1 MCF10A cells using a RUNX1 specific antibody (Fig. 2A). Enriched regions (peaks called by MACS2) were compared using k-means clustering (k=4) of normalized enrichment profiles of the three cell populations. This analysis revealed

subsets of genes that were either shared across the three groups or were specific for each, indicating dynamic binding of RUNX1 during and immediately after mitosis (Fig. 2A). Peak calling identified RUNX1 occupancy of both protein coding and long non-coding RNA (lncRNA) genes. Specifically, RUNX1 occupied 1070 genes in cell population not in G1 or M phase (Fig. 2A; green bar) and 1095 genes in G1-enriched cells (Fig. 2A; light red bar). Importantly, RUNX1 occupied 551 genes (413 protein coding and 138 lncRNAs) in mitotically enriched MCF10A cells (Fig. 2A; blue bar).

Functional relevance of RUNX1 occupancy in the three cell populations was determined by comparing RUNX1-occupied genes with those that are differentially regulated upon shRNA-mediated RUNX1 knockdown (39). Of the 1070 genes occupied by RUNX1 in cell populations not in G1 or M phases, 353 genes were deregulated upon RUNX1 depletion (Fig. 2A). Importantly, RUNX1 depletion deregulated 399 of 1268 RUNX1-bound genes in the M and G1 populations. These findings reveal that several hundred target genes are bookmarked by RUNX1 during mitosis and transcriptionally regulated in normal mammary epithelial cells.

To identify cellular processes and pathways that are comprised of RUNX1-bookmarked genes, we performed gene set enrichment analysis (GSEA) on genes bound by RUNX1 during mitosis or G1, or not bound in either cell cycle stage (Fig. 2B). Interestingly, most genes bookmarked by RUNX1 during mitosis were associated with negative regulation of gene expression and metabolic process (Fig. 2B; blue box). Consistent with a cellular requirement to reattach and enter the next cell cycle and fully resume transcription, genes bound during G1 were primarily enriched in biological processes involving cell anchorage, protein localization and positive regulation of gene

expression (Fig. 2B; red box). ChIP-seq results were further validated by motif analysis of RUNX1-bound peaks, which showed that the RUNX motif was the most enriched motif in all three cell populations (Fig. 2C). Importantly, RUNX1-bound genomic regions were also enriched in motifs for transcription factors (e.g., Fra1, JunB, ETS) known to cooperate with RUNX1 for gene regulation (74)(Fig. 2C). Together, these findings indicate that RUNX1 occupies genes involved in cell proliferation, growth, and phenotype during mitosis in normal mammary epithelial cells.

RUNX1 mitotically bookmarks RNA Pol I-transcribed genes that control cell growth

Our ChIP-Seq results revealed that RUNX1 occupies rDNA repeats in MCF10A mammary epithelial cells; all three MCF10A cell populations (Asynch, Mitotic and G1) exhibited significant fold enrichment within the promoter region of hrDNA (Fig. 3A), suggesting a potential role for RUNX1 in regulating rRNA genes in MCF10A cells. We confirmed this finding in actively proliferating MCF10A cells by immunofluorescence microscopy for antibodies specific against RUNX1 and upstream binding factor (UBF), a transcriptional activator that remains bound to rRNA genes during mitosis (75). We observed large RUNX1 foci colocalizing with UBF throughout each stage of mitosis (Fig 3B and Suppl. Fig. 4). Colocalization between RUNX1 and UBF was validated by confocal microscopy. Line scans of MCF10A cells show that although RUNX1 and UBF occupy distinct nuclear microenvironments in interphase (n=15), both proteins substantially colocalize in metaphase (n=15)(Suppl. Fig. 4). Taken together, these findings establish RUNX1 binding to ribosomal DNA repeat regions by ChIP-Seq (Fig. 3A) and confirmed at the cellular level by confocal microscopy (Fig 3B & Suppl. Fig. 4).

We experimentally addressed the hypothesis that RUNX1 regulates ribosomal RNA gene expression by using a pharmacological inhibitor of RUNX1. The small molecule inhibitor AI-14-91, which has been extensively characterized by several groups, interferes with RUNX1-CBFβ interaction and disrupts RUNX1 DNA binding (76, 77). We examined the effect of RUNX1 inhibitor on pre-rRNA expression and found that pre-rRNA expression was significantly increased at 12hr and 48hr time points after treatment of asynchronous cells with the specific RUNX1 inhibitor but not the control inactive compound AI-4-88, indicating that RUNX1 suppresses rRNA gene expression in normal mammary epithelial cells (Fig. 3C). Because levels of rRNA directly correlate with global protein synthesis, a fluorescent-based detection method was used to measure newly synthesized proteins. Cells treated with AI-14-91 for 24hr or 48hr showed a moderate change in levels of global protein synthesis in comparison to AI-4-88 control-treated cells under identical conditions (n=3; Fig. 3D). Together, our results demonstrate that RUNX1 bookmarks RNA Pol I regulated rRNA genes during mitosis and transcriptionally represses them during interphase with moderate impact on global protein synthesis in normal mammary epithelial cells.

RUNX1 occupies RNA Pol II-transcribed genes involved in hormone-responsiveness and cell phenotype during mitosis

Using RUNX1-bookmarked genes, gene set enrichment analysis (GSEA) was performed to identify regulatory pathways (Fig. 4A). In agreement with known roles of RUNX1 (78-82), the top 10 pathways identified were those involved in regulation of G2M Checkpoint, E2F targets, p53, and DNA repair (Fig. 4A). Consistent with our finding that

RUNX1 bookmarks and regulates rRNA genes, one of the pathways identified is mTOR signaling, a pathway that is required for cell growth and is a therapeutic target in breast cancers (83, 84). Relevant to the normal mammary epithelial phenotype, both early and late estrogen responsive gene sets significantly overlap with RUNX1 mitotically bookmarked genes (Fig. 4A). Because estrogen plays vital roles in promoting proliferative phenotypes of mammary epithelial cells (85-87), we interrogated RUNX1 bookmarked genes to identify those bound by RUNX1 and ERα in MCF7 cells, where RUNX1 contributes to higher order genome organization (Fig. 4B) (88, 89). Using publicly available datasets of ERα genome-wide occupancy and estradiol-regulated gene expression (GSE40129)(90), we find that a subset of genes mitotically bookmarked by RUNX1 is also bound by ERα, and either up or down regulated in response to estradiol. These findings indicate that RUNX1-bookmarked genes are involved in pathways that control hormone-responsiveness, proliferation and growth of normal mammary epithelial cells (Fig. 4B).

We identified a novel subset of genes that are bookmarked by RUNX1 and relate to regulatory pathways involved in cellular phenotype including TNFα, Apical Junction and Notch signaling (Fig. 4A). Furthermore, NEAT1 and MALAT1, lncRNAs often deregulated in breast cancer (91, 92), were also mitotically bookmarked by RUNX1. Of the 413 RUNX1 bookmarked protein coding genes, *TOP2A*, *MYC*, *HES1*, *RRAS*, *H2AFX*, and *CCND3* are representative of RNA Pol II-transcribed genes involved in phenotype maintenance and cell fate decisions (See Suppl. Table 1 for complete list). Recently, *HES1* and *H2AFX* have been identified as regulators of breast epithelial phenotype (93-95). In our ChIP-seq dataset, *HES1* and *H2AFX* show significant fold enrichment of

RUNX1 occupancy between the three populations of MCF10A cells (Fig. 4C; top panels). Expression of *HES1* increased upon inhibition of RUNX1 DNA binding (Fig. 4C; left panel—bar graph), indicating that RUNX1 represses *HES1*. In contrast, *H2AFX* expression at 24hr and 48hr of inhibitor treatment was decreased, suggesting RUNX1 activates H2AFX expression (Fig. 4C; right panel—bar graph). These results suggest that RUNX1 bookmarks both protein coding and non-coding genes that are critical determinants of epithelial lineage identity as a potential mechanism to stabilize the mammary epithelial phenotype.

Inhibition of RUNX1 DNA binding causes epithelial to mesenchymal transition and alters the associated transcriptome

To experimentally address whether disruption of RUNX1 bookmarking leads to a change in epithelial phenotype, we treated cells with RUNX1 DNA binding inhibitor and the inactive control compound and monitored changes in cell morphology (Fig. 5A). Consistent with RUNX1 bookmarking and regulation of genes critical for epithelial phenotype (Figs. 2 & 4), disruption of RUNX1 DNA binding for 48 hours resulted in mesenchymal morphology. We next examined whether long-term inhibition of RUNX1 caused a permanent change in cell phenotype. Longer term treatment (5 days) of actively proliferating MCF10A cells showed significant apoptosis, although a small sub-population of cells survived and exhibited an altered phenotype (Fig. 5B). The surviving sub-population at day 5 was recovered by culturing cells in media without the inhibitor. By day 3-4 following media replacement, cells clearly showed a mesenchymal morphology (Fig. 5B), indicating that interfering with RUNX1 DNA binding causes loss of the normal

mammary epithelial phenotype. Consistent with changes in cell morphology, we find alterations in expression and localization of the cytoskeletal F-actin protein (Fig. 5C). These observations were confirmed by examining the expression of epithelial markers (e.g., E-cadherin (Fig. 5D)), as well as mesenchymal markers (e.g., Vimentin (Fig. 5D)). E-cadherin was largely unchanged; however, Vimentin expression was significantly increased, confirming an epithelial-to-mesenchymal transition upon inhibition of the RUNX1-CBFβ interaction.

To identify transcriptome-wide changes associated with EMT upon inhibition of RUNX1 DNA binding activity that is required for retention of the protein with mitotic chromosomes (56), we performed RNA sequencing (in triplicates) at each of the indicated time points (Day 1 and 2 in Crisis Phase and Day 4 and 7 in Recovery Phase). Heatmap analysis of all time points identified substantial changes in gene expression as cells transition from epithelial to mesenchymal phenotype (Fig. 6A). A differential gene expression analysis between the crisis and recovery phases uncovered significant changes in expression of genes associated with EMT (e.g., IL32, SERPINB2 etc.; Fig. 6B). Importantly, a subset of differentially expressed genes was occupied by RUNX1 during mitosis. We performed pathway analysis on differentially expressed genes (Fig. 6C and Suppl. Table 2). Consistent with phenotypic changes, we found that multiple signaling pathways that include TNF alpha, Interferon Gamma and estrogen responsiveness were altered during EMT caused by RUNX1 inhibition.

We next determined the effect of the inhibition of RUNX1-CBFβ interaction on mitotic retention of the protein. Actively proliferating MCF10A cells were treated with the inhibitor (AI-14-91) for 6hr, 12hr, 24hr, and 48hr at 20μM; a structurally similar but inactive

compound (AI-4-88) was used as a control under identical conditions. Cells were subjected to immunofluorescence microscopy followed by detection of RUNX1 and UBF as described above. Although RUNX1 signal was detected in all mitotic sub-stages (Suppl. Fig. 5), we observed a substantial decrease in RUNX1 signal intensity on metaphase chromosomes (white arrows; Fig. 6D), indicating that RUNX1-CBFβ interaction and RUNX1 DNA binding activity play a key role in mitotic gene bookmarking. These changes were more pronounced for smaller RUNX1 foci and were not observed in control-treated cells; appreciable signal for large RUNX1 foci that colocalize with UBF (Fig. 3B & Suppl. Fig. 4) remained detectable in all sub-stages of mitosis (Fig. 6D and Suppl. Fig. 5). Together, these findings indicate that RUNX1 mitotic bookmarking of genes related to epithelial cell growth, proliferation, and lineage is associated with epithelial cell identity, and disruption of RUNX1 DNA binding leads to mesenchymal transition.

DISCUSSION

This study identifies retention of RUNX1 on mitotic chromosomes and occupancy of target genes as a potential epigenetic mechanism for coordinate regulation of RNA Pol I- and II-transcribed genes that are critical for mammary epithelial proliferation, growth, and phenotype maintenance. Pharmacological inhibition of RUNX1 DNA binding causes transition of mammary epithelial cells to a mesenchymal phenotype, indicating that RUNX1 bookmarking of target genes contributes to stabilizing the normal breast epithelial phenotype.

Our findings are the first to examine RUNX1 bookmarking of target genes during mitosis in mammary epithelial cells and to report that RUNX1 coordinately controls cell growth-related ribosomal RNA (rRNA) genes and a large subset of cell proliferation/phenotype-related genes in these cells. One target gene of interest is hairy and enhancer of split-1 (*HES1*). Hes1 is a transcription factor that represses genes involved in cellular development and is regulated primarily by NOTCH signaling, one of our top ten overlapping hallmark gene sets bookmarked by RUNX1 (Fig. 4)(96, 97). HES1 was recently shown to have a prominent role in proliferation and invasion of breast cancer cells, and its silencing led to downregulation of p-Akt signaling and ultimately prevented EMT (93). Our findings indicate that RUNX1 stabilizes the normal mammary epithelial phenotype, in part, by bookmarking *HES1* and suppressing its expression.

Another important RNA Pol II-transcribed gene mitotically bookmarked by RUNX1 and critical for maintaining cellular phenotype is histone variant H2AFX (*H2AFX*). Silencing *H2AFX* in breast epithelial cells leads to induction of EMT through activation of *SNAIL2/SLUG* and *TWIST1* (95). Upon inhibition of the RUNX1-CBFβ interaction, we find

a decrease in *H2AFX* expression and a concomitant, significant increase in SNAIL2/SLUG expression. These data identify RUNX1 as a novel upstream regulator of *H2AFX* expression; RUNX1 bookmarking and activation of H2AFX and subsequent suppression of *SNAIL2/SLUG* prevents EMT in breast epithelial cells.

Several groups have shown that RUNX1 interacts with ERα at both enhancer regions and transcriptional start sites (TSSs) for regulation of specific genes (34, 88). Our ChIP-Seq results, coupled with publicly available data sets, reveal a novel finding: RUNX1 bookmarking of a subset of ERα-occupied, hormone-responsive genes during mitosis may be critical for maintenance of the breast epithelial phenotype. Future studies will be required to investigate mechanistic significance of this observation in estrogen receptor positive mammary epithelial and breast cancer cells.

Our findings suggest that mitotic gene bookmarking by RUNX1 contributes to regulation of the mammary epithelial phenotype. Equally important, our study shows that inhibition of RUNX1 DNA binding specifically elicits an epithelial-to-mesenchymal transition that accompanies changes in critical genes and pathways involved in EMT. These findings are further supported by RUNX1 mitotic occupancy of cell growth-related rRNA genes, and together highlight a key role of RUNX1 in coordinating cell proliferation, growth and phenotype. Because RUNX1 interacts with multiple co-activators and co-repressors, additional in-depth studies are required to determine contributions of RUNX1 co-regulatory proteins to mitotic gene bookmarking.

Another novel contribution of the current study is mitotic bookmarking of lncRNAs by a transcription factor. RUNX1 was recently shown to regulate lncRNAs NEAT1 and MALAT1 (89, 91), which have critical roles in the onset and progression of breast cancer

(92). Our findings show that, in addition to occupying protein coding genes, RUNX1 bookmarks several lncRNAs for post-mitotic regulation. It will be important to determine if RUNX1-bookmarked lncRNAs have G1-specific roles in maintaining the normal mammary epithelial phenotype and/or in the onset and progression of breast cancer.

In summary, this study shows that RUNX1 occupies RNA Pol I- and II-transcribed genes during mitosis for coordinate regulation of normal mammary epithelial proliferation, growth, and phenotype. Disruption of RUNX1 DNA binding leads to the epithelial-to-mesenchymal transition, a key event in breast cancer onset, and implicates RUNX1 mitotic gene bookmarking as an epigenetic mechanism to physiologically sustain the mammary epithelial phenotype.

MATERIALS AND METHODS

Cell Culture Techniques

Breast epithelial (MCF10A) cells were cultured in DMEM/F-12 50/50 mixture (Corning™, Corning, NY). Culturing media was also supplemented with horse serum to 5% (GIBCO, Grand Island, NY), human insulin to 10µg/mL (Sigma Aldrich, St. Louis, MO), human epidermal growth factor to 20ng/mL (PeproTech, Rocky Hill, NJ), cholera toxin to 100ng/mL (Thomas Scientific, Swedesboro, NJ), hydrocortisone to 500ng/mL (Sigma Aldrich, St. Louis, MO), Penicillin-Streptomycin to 100U/mL (Thermo Fisher Scientific, Ashville, NC), and L-Glutamine to 2mM (Thermo Fisher Scientific, Ashville, NC).

For mitotic arrest of parental MCF10A cells, culturing media was supplemented with 50ng/mL of Nocodazole (Sigma Aldrich, St. Louis, MO) and incubated with cells for 16hrs. Supplementing culturing media with equivalent volumes of DMSO (Sigma Aldrich, St. Louis, MO) served as a control. DMSO-treated and mitotically arrested populations of MCF10A cells were harvested following the 16hr incubation. For G1 (released from mitotic arrest) populations of MCF10A cells, the nocodazole-supplemented media was replaced with normal media and cells were incubated for 3hrs, after which the released cell population was harvested for subsequent analyses that include western blotting, qPCR, FACS and ChIP-seq.

Western Blot Analyses

Protein lysates were prepared by incubating cells in RIPA buffer on ice for 30min, followed by sonication using Q700 Sonicator (QSonica, Newtown, CT). Proteins were resolved by SDS-PAGE and transferred to PVDF membrane using standard protocols.

Following primary antibodies were used at a 1:1000 dilution (except Lamin B, which was used at 1:2000 dilution) in this study: UBF (sc-13125, Santa Cruz Biotechnology, Dallas, TX); RUNX1 (4334S, Cell Signaling Technologies, Danvers, MA); Cyclin B (4138S, Cell Signaling Technologies, Danvers, MA); Beta-Actin (3700S, Cell Signaling Technologies, Danvers, MA), and CDT1 (ab70829, AbCam, Cambridge, UK); Lamin B1 (ab16048, AbCam, Cambridge, UK). Horseradish peroxidase conjugated secondary antibodies used in this studies were: goat anti-mouse IgG at 1:5000 dilution (31460, Invitrogen, Carlsbad, CA), goat anti-rabbit IgG HRP conjugated (31430, Thermo Fisher Scientific, Ashville, NC) at 1:1000, 1:2000, or 1:5000 dilutions. Blots were developed using Clarity Western ECL Substrate (Bio-Rad, Hercules, CA) and imaged using Molecular Imager® Chemi doc™ XRS+ Imaging System (Bio-Rad, Hercules, CA) aided by Image Lab Software Version 5.1 (Bio-Rad, Hercules, CA).

Confocal Microscopy, Image Acquisition, Processing and Analyses

MCF10A cells were plated on gelatin-coated coverslips in 6-well plates at 175,000 cells/mL and processed for immunofluorescence 24 hrs after plating using standard protocol. Briefly, cells were washed twice with sterile-filtered PBS on ice and cell were fixed in 1% MeOH-free Formaldehyde in PBS for 10min. After permeabilization in 0.25% Triton X-100-PBS solution, cells were sequentially incubated with primary and Alexa fluorophore conjugated secondary antibodies for 1hr each at 37℃ in a humidified chamber with extensive washes after each incubation. Primary antibodies used were: RUNX1 at 1:10 dilution (4334S, Cell Signaling Technologies, Danvers, MA), and Upstream Binding Transcription Factor (UBF) at 1:200 dilution (F-9 sc-13125, Santa Cruz

Biotechnology, Dallas, TX). Secondary antibodies used were goat anti-rabbit IgG conjugated with Alexa Fluor 488 (A-11070, Life Technologies, Carlsbad, CA) and goat anti-mouse IgG conjugated with Alexa Fluor 594 (A-11005, Life Technologies, Carlsbad, CA) diluted 1:800. Cells were counterstained with DAPI to visualize DNA and coverslips were mounted onto slides in ProLong Gold Antifade Mountant (Thermo Fisher Scientific, Ashville, NC). Images were captured using a Zeiss Axio Imager.Z2 fluorescent microscope and Hamamatsu ORCA-R2 C10600 digital camera. Images were processed using ZEN 2012 software.

To examine mitotic localization of RUNX1 in unfixed cells, an expression plasmid containing RUNX1-EGFP was introduced using either nucleofection or Lipofectamine 2000 transfection reagent in actively proliferating MCF10A cells grown on gelatin-coated coverslips. After 16 hours of nucleofection, cells were washed once with 1X PBS and stained with Hoechst dye to visualized DNA. Coverslips were mounted using the ProLong Gold Antifade Mountant and subjected to confocal microscopy.

Cells were initially imaged with a Zeiss LSM 510 META confocal laser scanning microscope (Carl Zeiss Microscopy, LLC., Thornwood, NY, USA). The DAPI signal was excited with a 405 nm laser and collected with a 425-475 nm band pass filter, Alexa 488 was excited with a 488 nm laser and collected with a 500-550 nm band pass filter, and Alexa 568 with a 561 nm laser and collected with a 570-620 nm band pass filter. Images were captured with a Plan-Fluor 40X (1.3 NA) objective lens. The confocal pinhole was initially set to 1.2 Airy Unit diameter for the 561 nm excitation giving an optical section thickness of 0.41 µm. Images were acquired at 12-bit data depth, and all settings, including laser power, amplifier gain, and amplifier offset were established using a look

up table to provide an optimal gray-scale intensities. All images were acquired using matching imaging parameters. The acquired images were subjected to colocalization analysis via Volocity version 6.3.0 (Perkin Elmer, Waltham, MA, USA). At least 15 interphase and 15 metaphase cells were identified in captured images and appropriate thresholds were manually determined to eliminate background fluorescence for calculating Pearsons and Manders correlation coefficients between RUNX1 and UBF.

To ensure the specificity of our observations, additional samples were imaged with a Nikon A1R-ER laser scanning confocal microscope (Nikon, Melville, NY, USA). Images were acquired with the galvano scanner at a frame size of 1024 X 1024 pixels with an Apo TIRF 60X objective lens (N.A. 1.49) zoom of 2 and 1.2 Airy Unit pinhole setting. Images were also viewed in NIS Elements version 5.02.01 and analyzed using the line profiling tool. Overlaying DAPI, RUNX1, and UBF fluorescent intensities from individual channels along the line profile revealed overlapping peak intensities between the RUNX1 and UBF channels, thus indicating colocalization.

RNA Isolation, cDNA Synthesis and Quantitative PCR

Total RNA was isolated from MCF10A cells using TRIzol™ Reagent (Invitrogen, Carlsbad, CA) and Direct-Zol™ RNA MiniPrep isolation kit (Zymo Research, Irvine, CA) following manufacturer instructions. cDNA was created using SuperScript IV® First-Strand Synthesis System for RT-PCR (ThermoFisher, Asheville, NC). Resulting samples were quantified on a Qubit 2.0 Fluorometer (Invitrogen, Carlsbad, CA) and diluted to 500pg/μL. Equal amounts of DNA template were loaded for samples analyzed by qPCR. At least three independent biological replicates were analyzed for expression of RUNX1

bookmarked genes by qPCR. Student's t-test was used to determine the significance of changes in transcript levels under different biological conditions.

Chromatin Immunoprecipitation, Library Preparation, Sequencing and Bioinformatics Analyses

Asynchronous (Asynch), mitotically arrested (M), and released from mitosis (G1) MCF10A breast epithelial cells were subjected to chromatin immunoprecipitation using a modified Farnahm' protocol {O'Geen, 2010 #2713}. Sonication parameters for each population of cells was as follows: Peak Watt 140W, Duty Factor 10, Cycle/Burst 200 using a S220 focused ultra-sonicator (Covaris, Matthews, NC). M and G1 populations of cells were sonicated for 28min total, whereas asynchronous populations of cells were sonicated for 36min. An aliquot of sonicated lysates was boiled in 100^{o}C for 15min with NaCl and elution buffer and DNA was purified using PureLink^{TM} PCR Purification Kit (K310001, ThermoFisher, Ashville, NC). Purified DNA was resolved on a 1.5% agarose gel to confirm optimal sonication (bulk of fragments between 200-400bp) prior to performing ChIP. In parallel, an aliquot was also quantified via Qubit 2.0 Fluorometer (Invitrogen, Carlsbad, CA) and analyzed by using a High Sensitivity DNA Kit on a Bioanalyzer 2100 (Agilent, Santa Clara, CA).

For chromatin immunoprecipitation (ChIP) reactions, 150ug of sonicated chromatin was incubated with 10ug of RUNX1 antibody (4336BF, Cell Signaling Technologies, Danvers, MA), diluted 1:10 in IP dilution buffer, and incubated overnight (16-18hrs) at 4^{o}C with mild agitation. Following incubation, 150uL of Protein A/G magnetic beads (Thermo Scientific – Pierce, Waltham, MA) per ug of antibody used were added to

each IP reaction and incubated for 2-4hrs at 4°C with mild agitation. Beads were extensively washed with IP wash buffers and resuspended in Elution Buffer to extract immunoprecipitated chromatin, which was subsequently purified using PureLink™ PCR Purification Kit. At least 3 biological replicates were performed for each cell population and each antibody.

ChIP libraries were generated using Accel-NGS® 2S Plus DNA Library kit (Swift Biosciences, Ann Arbor, MI) following manufacturers protocol. Input and RUNX1 ChIP samples were normalized to 1ng prior to library generation. Libraries were amplified in an optional PCR step for 12 total cycles. Finalized libraries were double size selected using AMPure XP beads (0.8X and 0.2X volume ratios to sample), resulting in the majority fragments sized between 250-400bp. Next generation sequencing of pooled ChIP libraries was performed by the University of Vermont Cancer Center - Vermont Integrated Genomics Resource (VIGR).

Single end, 50bp reads (SE50) were processed pre-alignment by removing adapter reads (Cutadapt v1.6) and trimming low quality base calls from both ends (FASTQ Quality Trimmer 1.0.0; min score >= 20, window of 10, and step size of 1). Because we were specifically investigating rDNA, a customized build of hg38 was constructed that included normally masked regions of rDNA (Gencode U13369). Since some (although not complete) rDNA sequence is present in the hg38 assembly, we masked all parts of hg38 that would normally be attributed to rDNA sequences (bedtools v2.25.0 maskfasta) based on alignment positions of 50 bp *in silico* reads generated across U13369. Finally, we appended the complete rDNA sequence as a distinct

sequence (chrU13369.1) to the masked hg38 FASTA resulting in the hg38_rDNA assembly used for analysis.

Resulting reads were aligned to hg38_rDNA (STAR v2.4; splicing disabled with '--alignIntronMax 1'). Next, we called peaks and generated fold-enrichment (FE) bedGraph files (MACS2 v2.1.0.20140616; callpeak at p-value e-5; and bdgcmp with FE method)(98). Irreproducible Discovery Rate (IDR) was conducted using unpooled replicates with all peaks in pooled samples passing an IDR cutoff of 0.5 (99). To reduce artificial peaks, we calculated strand cross-correlation for all peaks at a shift of 95 bp (the mean observed fragment size of 180 bp minus the read size of 85bp) and unshifted (100). We eliminated peaks that exhibited low shifted correlation (shifted correlation <0.7) and those that exhibited high unshifted correlation relative to shifted (shifted – unshifted correlation < 0.1). This increased retrieval of the RUNX1 motif and improved agreement with other RUNX1 datasets. Passing peaks were annotated separately to mRNA and lncRNA transcript start sites (TSSs) using Gencode v27 with a distance cutoff of 5000 bp. Regional distribution of peaks was determined using the same annotation reference limited to the “basic” tag for exons and promoters.

Inhibitor Treatment and Assessment of Global Protein Synthesis

Core binding factor – Beta (CBFβ) inhibitors AI-4-88 and AI-14-91 were kindly provided by John H. Bushweller (University of Virginia) and used to evaluate RUNX1 DNA-binding inhibition in MCF10A cells. Protein synthesis evaluation by immunofluorescence was conducted following manufacturer protocol (K715-100, BioVision, San Francisco, CA). To examine effects of inhibiting the RUNX1-CBFβ

interaction, MCF10A cells were treated with active or inactive compound for 48 hours. Culture medium containing the active or inactive compounds was replaced with fresh medium without the compounds and cells were harvested 4- and 7-days post medium change.

RNA-Sequencing, Differential Expression Analysis, and Pathway Analysis:

RNA was isolated using Direct-zol RNA MiniPrep (Zymo Research, Irvine, CA, USA) and was quantified and assayed for RNA integrity by Bioanalyzer (Agilent Technologies, Inc., Santa Clara, CA, USA). Following the removal of ribosomal RNA, the RNA pool was reverse transcribed, amplified, purified, and bound to strand-specific adaptors following the manufacturer's protocol (SMARTer Stranded Total RNA Sample Prep Kit, Takara Bio, Mountain View, CA, USA). cDNA libraries were assayed for quality control by Bioanalyzer (Agilent Technologies, Inc., Santa Clara, CA, USA). After cDNA quality validation, generated libraries were sequenced. 24 hour and 48-hour counts were grouped together into one "crisis" category and the day 4 recovery and day 7 recovery counts were grouped together into one "recovery" category. Treatment groups were compared with untreated MCF10A cells. After demultiplexing and quality filtering, reads were aligned to hg38 using Gencode (GRCh38.p13). As a reference, annotation with STAR (v2.5.2a)(101) aligned reads were then counted using HT-Seq (102). Differential gene expression was analyzed using DESeq2 in R v.3.5.1 (103). Parameters for significant differential expression were base mean expression greater than five, absolute log2 fold change greater than one, and a p-value less than 0.05. Pathway analysis was

533 performed using Gene Set Enrichment Analysis v6.3 (Broad Institute, Inc., MIT, UC San
534 Diego).
535
536 **ACKNOWLEDGEMENTS**
537 The authors thank Dr. Prachi Ghule, Department of Biochemistry, University of
538 Vermont for assistance in confocal microscopy, Scott Tighe, Pheobe Kehoe, and Jessica
539 Hoffman of the Vermont Integrative Genomics Resource for performing next generation
540 sequencing of samples, Dr. Roxana del Rio-Guerra of the Flow Cytometry and Cell
541 Sorting Facility for analysis of samples by FACS and Dr. Alan Howe, Department of
542 Pharmacology, University of Vermont, for providing Phalloidin reagent used in
543 immunofluorescence microscopy experiments.
544
545 **COMPETING INTERESTS**
546 No competing interests declared.
547
548 **FUNDING**
549 This work was supported by NIH grants P01 CA082834 (GSS & JLS), U01
550 CA196383 (JLS), U54 GM115516 (GSS), F32 CA220935 (to A.J. Fritz), and the Charlotte
551 Perelman Fund for Cancer Research (GSS). The confocal microscopy work described in
552 this manuscript was supported by Award Number 1S10RR019246 from the National
553 Center for Research Resources for purchase of the Zeiss 510 META confocal scanning
554 laser microscope and NIH award number 1S10OD025030-01 for purchase of the Nikon
555 A1R-ER point scanning confocal microscope from the National Center for Research

Resources. FACS experiments performed at the Harry Hood Bassett Flow Cytometry and Cell Sorting Facility, University of Vermont College of Medicine were supported by NIH S10-ODO18175.

DATA AVAILABILITY

GEO accession number for the sequencing data generated in this study is GSE121370.

FIGURE LEGENDS

Figure 1. RUNX1 associates with DNA during interphase and remains bound throughout mitosis in the form of major and minor foci. Representative immunofluorescent images of interphase and mitotic MCF10A breast epithelial cells showing subcellular localization of RUNX1, identified using a specific antibody, throughout mitosis. Mitotic cells were further classified into substages of mitosis based on DAPI topology. RUNX1 – Green (top row), DAPI – Blue (second row from top). Merged channel images (third row from top) contain an outlined region magnified in the bottom row labeled “inset”. White arrows highlight major Runx1 foci on mitotic chromatin. Three independent biological replicates were performed, and at least 20 cells for each mitotic substage were analyzed.

Figure 2. RUNX1 occupies protein coding genes and long non-coding RNAs across asynchronous, mitotic, and G1 populations of MCF10A breast epithelial cells. A) Heatmaps showing peaks called between A, M, and G1 MCF10A cells (left, middle, and right respectively). Cumulative occupancy of RUNX1 is shown as line graphs and genes that occupied by RUNX1 in each of the three cell populations are shown. Shown also are genes that are deregulated upon RUNX1 downregulation. For example, 1070 genes are bound by RUNX1 in cells that are neither in M nor G1 cells (green bar graph) and of those, 353 genes are deregulation upon RUNX1 deregulation. B) Gene ontology analysis of RUNX1-bound genes identifies key regulatory pathways that are similar or unique in the three cell populations. C) Motif analysis of A, M, and G1 MCF10A cells reveals RUNX motif as one of the top motifs in all cell populations.

586 Binding sites for key transcription factors that are known to cooperate with RUNX1 are
587 also identified.

588 **Figure 3. RUNX1 bookmarks rDNA promoter repeat regions and affects both pre-**
589 **rRNA and global protein expression.** A) ChIP-Seq tracks of A, M, and G1 (top,
590 middle, bottom respectively) MCF10A cells mapped against rDNA repeat regions. B) A
591 representative metaphase MCF10A cell, stained for RUNX1 (green) and UBF1 (red)
592 localization, is shown demonstrating that the two proteins colocalize during mitosis
593 (merged). Cells are also counter stained with DAPI to visualize DNA (blue) and identify
594 mitosis substages. C) qRT-PCR data of pre-rRNA in actively proliferating MCF10A cells
595 treated with either active (AI-14-91) or inactive (AI-4-88) compounds for 6, 12, 24, or
596 48hrs. Expression of pre-rRNA was normalized relative to Beta Actin expression. Graph
597 represents three independent biological replicates. Asterisks represents a *p* value of
598 <0.05. D) Representative fluorescence microscopy images of global protein synthesis
599 from MCF10A cells treated with either AI-4-88 (left) or AI-14-91 (right) for 24hr at 20μM
600 (n=2). Intensity of red fluorescence at 580nm emission indicates nascent protein
601 synthesis. All images were taken with 1000ms exposures.

602 **Figure 4. RUNX1 bookmarks RNA Pol II-transcribed genes involved in**
603 **maintenance of breast epithelial phenotype.** A) Gene Set Enrichment (GSE) analysis
604 from interrogating mitotically bookmarked genes (i.e. RUNX1 mitotically occupied)
605 against Hallmark Gene sets from Molecular Signatures Database (MSigDB). The top 10
606 most significantly overlapping gene sets are shown from top to bottom. B) Scatter plot of
607 genes identified to be up or down regulated in response to estradiol treatment, that are
608 also bound by estrogen receptor α (ERα) and RUNX1 (empty circles, blue for

downregulated and red for upregulated). Scatter plot also illustrates up or down regulated genes in response to estradiol treatment that are bound by ERα and mitotically bookmarked by RUNX1 (filled in circles, blue for downregulated and red for upregulated). C) Top panel: ChIP-Seq tracks of *HES1* (left) and *H2AFX* (right) from asynchronous (top-red), mitotic (middle-green), and G1 (bottom-blue). Bottom panel: qRT-PCR data of *HES1* (left) and *H2AFX* (right) in asynchronous MCF10A cells treated with either active (AI-14-91) or inactive (AI-4-88) inhibitors for 6hr, 12hr, 24hr and 48hr at 20μM. Expression of target genes were normalized relative to beta actin.

Figure 5. Disrupting RUNX1 mitotic gene bookmarking in MCF10A cells leads to a transformed cellular phenotype and EMT.

A) Phase contrast microscopy images of MCF10A cells treated with AI-4-88 or A-14-91 for 48 hours at 20μM. Left panel – 20X magnification, right panel – 40X magnification. The outlines rectangle in the left panel is the resulting 40X magnification in the right panel. B) Top panel: Experimental schematic depicting treatment schedule for the "crisis" and "recovery" stages. Bottom panel: Phase contrast microscopy images from Day 0, 1, and 2 or crisis where MCF10A cells were treated with AI-14-91 at 20μM (top – left, middle, right respectively). Phase contrast images from Day 0, 4, and 7 or recovery following a media replacement. C) Morphological changes upon inhibition of the cytoskeletal protein F-actin. When compared to inactive compound (left panel), cells treated with the active compound show substantial alteration in cytoarchitecture (right panel). D) Western blot for RUNX1, RUNX2, epithelial marker E-cadherin, mesenchymal marker Vimentin, and loading control Beta-actin (top panel to bottom

631 panel respectively) in MCF10A whole cell lysate harvested from the crisis 24 hour and
632 48-hour timepoints and recovery day 4 and day 7 timepoints.

633 **Figure 6. Differential expression and pathway analysis of RNA-Seq shows**
634 **changes in key regulatory pathways involved in cell proliferation, metabolism,**
635 **cell cycle control, estrogen response, and EMT.** A) Expression heatmap of three
636 biological replicates of 24-hour and 48-hour crisis timepoints and Day 4 and Day 7
637 recovery timepoints. B) Scatterplot of log2 fold change between crisis and recovery
638 phases. Most changed genes in each stage are indicated. C) Table of overlapping
639 pathways specific to crisis and recovery stages. D) Representative immunofluorescence
640 images of the active compound (AI-14-91)-treated MCF10A cells in prophase and
641 metaphase are shown. A substantial decrease in smaller RUNX1 foci (green) during
642 mitosis is observed when compared to the inactive (AI-4-88) compound. Large RUNX1
643 foci that colocalize with UBF (red) are detectable at all substages of mitosis (white
644 arrows) in the presence of either active or inactive compounds.

645 **Supplementary Figure 1. Secondary antibody controls for immunofluorescence**
646 **microscopy.** To ensure the specificity of RUNX1 signal on mitotic chromosomes,
647 actively proliferating mammary epithelial MCF10A cells, grown on gelatin-coated
648 coverslips, were subjected to immunofluorescence microscopy procedure as described
649 in Materials and Methods section with one modification: no primary antibody was added,
650 but secondary antibodies were used at the same dilution as in all IF experiments. Nuclei
651 were counterstained with DAPI. Two different fields are shown, confirming that the
652 RUNX1 signal we observe on mitotic chromosomes is specific.

Supplementary Figure 2. RUNX1 associates with chromosomes during all stages of mitosis in unfixed live MCF10A cells. Mammary epithelial MCF10A cells were transiently transfected with EGFP-RUNX1 and imaged by confocal microscopy without fixation (see Materials and Methods section for details). Top panels show RUNX1 (green) association with mitotic chromosomes in unfixed, live MCF10A cells. Cells were counterstained with Hoechst (middle panels; blue) to visualize DNA in live cells and to identify mitotic cells. Merged images (bottom panels) were generated to confirm localization of RUNX1 signal with DNA. Arrow heads indicate punctate RUNX1 foci retained on mitotic chromosomes.

Supplementary Figure 3. Determination of optimal nocodazole dosage for maximum mitotic block. A) Micrographs of MCF10A cells, treated with various doses of nocdazole for 16 hours, are shown (bottom panels). DMSO control treatment is also included (top panels). B) Experimental schematic depicting mitotic arrest and harvest of each treated MCF10A cell population: Asynchronous – A, Mitotic – M, and Released – G1. C) Western blot of each harvested MCF10A population for cell cycle specific markers to evaluate mitotic arrest and synchronization procedure. D) Fluorescence-activated cell sorting (FACS) analysis of harvested A, M, and G1 MCF10A populations to determine mitotic purity and DNA content (n=2 biological replicates per group).

Supplementary Figure 4. RUNX1 colocalizes with RNA Pol I subunit, upstream binding factor (UBF) on mitotic chromatin. A) Immunofluorescence microscopy images of RUNX1 (green – top row), UBF (red – 2nd row from top), DAPI (blue – 2nd row from bottom), and the three channels merged (bottom row) in MCF10A cells. Images were captured of spontaneously dividing MCF10A cells in different substages of mitosis.

B) Representative images of line profiles taken on interphase vs metaphase cells (n=15 each).

Supplementary Figure 5. The RUNX1-CBFβ inhibitor reduces RUNX1 association with mitotic chromosomes. MCF10A cells, treated with 20μM inactive control compound or active inhibitor for 12 hours, were stained for localization of endogenous RUNX1 (green) to mitotic chromosomes. RUNX1 retention on mitotic chromosomes, particularly in smaller foci, was substantially reduced in cells treated with active inhibitor of RUNX1-CBFβ interaction, which disrupts RUNX1 DNA binding activity.

Dataset S1 (separate file). List of genes occupied by RUNX1 in asynchronous, mitotic and G1 cell populations in mammary epithelial cells.

Dataset S2 (separate file). Gene enrichment analysis of genes sensitive to RUNX1-CBFβ inhibition during crisis and recovery phases of epithelial to mesenchymal transition in MCF10A cells.

690 **REFERENCES**

691 1. Banerji S, Cibulskis K, Rangel-Escareno C, Brown KK, Carter SL, Frederick AM,
692 Lawrence MS, Sivachenko AY, Sougnez C, Zou L, Cortes ML, Fernandez-Lopez JC,
693 Peng S, Ardlie KG, Auclair D, Bautista-Pina V, Duke F, Francis J, Jung J, Maffuz-Aziz
694 A, Onofrio RC, Parkin M, Pho NH, Quintanar-Jurado V, Ramos AH, Rebollar-Vega R,
695 Rodriguez-Cuevas S, Romero-Cordoba SL, Schumacher SE, Stransky N, Thompson
696 KM, Uribe-Figueroa L, Baselga J, Beroukhim R, Polyak K, Sgroi DC, Richardson AL,
697 Jimenez-Sanchez G, Lander ES, Gabriel SB, Garraway LA, Golub TR, Melendez-
698 Zajgla J, Toker A, Getz G, Hidalgo-Miranda A, Meyerson M. 2012. Sequence analysis
699 of mutations and translocations across breast cancer subtypes. Nature 486:405-9.
700 2. Ciriello G, Gatza ML, Beck AH, Wilkerson MD, Rhie SK, Pastore A, Zhang H,
701 McLellan M, Yau C, Kandoth C, Bowlby R, Shen H, Hayat S, Fieldhouse R, Lester SC,
702 Tse GM, Factor RE, Collins LC, Allison KH, Chen YY, Jensen K, Johnson NB,
703 Oesterreich S, Mills GB, Cherniack AD, Robertson G, Benz C, Sander C, Laird PW,
704 Hoadley KA, King TA, Network TR, Perou CM. 2015. Comprehensive Molecular
705 Portraits of Invasive Lobular Breast Cancer. Cell 163:506-19.
706 3. Elsheikh SE, Green AR, Rakha EA, Powe DG, Ahmed RA, Collins HM, Soria D,
707 Garibaldi JM, Paish CE, Ammar AA, Grainge MJ, Ball GR, Abdelghany MK, Martinez-
708 Pomares L, Heery DM, Ellis IO. 2009. Global histone modifications in breast cancer
709 correlate with tumor phenotypes, prognostic factors, and patient outcome. Cancer Res
710 69:3802-9.
711 4. Li Z, Herold T, He C, Valk PJ, Chen P, Jurinovic V, Mansmann U, Radmacher
712 MD, Maharry KS, Sun M, Yang X, Huang H, Jiang X, Sauerland MC, Buchner T,

713 Hiddemann W, Elkahloun A, Neilly MB, Zhang Y, Larson RA, Le Beau MM, Caligiuri
714 MA, Dohner K, Bullinger L, Liu PP, Delwel R, Marcucci G, Lowenberg B, Bloomfield
715 CD, Rowley JD, Bohlander SK, Chen J. 2013. Identification of a 24-gene prognostic
716 signature that improves the European LeukemiaNet risk classification of acute myeloid
717 leukemia: an international collaborative study. J Clin Oncol 31:1172-81.
718 5. Widschwendter M, Jones PA. 2002. DNA methylation and breast carcinogenesis.
719 Oncogene 21:5462-82.
720 6. Zhang M, Lee AV, Rosen JM. 2017. The Cellular Origin and Evolution of Breast
721 Cancer. Cold Spring Harb Perspect Med 7.
722 7. Chen T, You Y, Jiang H, Wang ZZ. 2017. Epithelial-mesenchymal transition
723 (EMT): A biological process in the development, stem cell differentiation, and
724 tumorigenesis. J Cell Physiol 232:3261-3272.
725 8. Kalluri R, Weinberg RA. 2009. The basics of epithelial-mesenchymal transition. J
726 Clin Invest 119:1420-8.
727 9. Nieto MA. 2013. Epithelial plasticity: a common theme in embryonic and cancer
728 cells. Science 342:1234850.
729 10. Prieto-Garcia E, Diaz-Garcia CV, Garcia-Ruiz I, Agullo-Ortuno MT. 2017.
730 Epithelial-to-mesenchymal transition in tumor progression. Med Oncol 34:122.
731 11. Suarez-Carmona M, Lesage J, Cataldo D, Gilles C. 2017. EMT and
732 inflammation: inseparable actors of cancer progression. Mol Oncol 11:805-823.
733 12. Thiery JP, Acloque H, Huang RY, Nieto MA. 2009. Epithelial-mesenchymal
734 transitions in development and disease. Cell 139:871-90.

735 13. Micalizzi DS, Farabaugh SM, Ford HL. 2010. Epithelial-mesenchymal transition
736 in cancer: parallels between normal development and tumor progression. J Mammary
737 Gland Biol Neoplasia 15:117-34.
738 14. Schmalhofer O, Brabletz S, Brabletz T. 2009. E-cadherin, beta-catenin, and
739 ZEB1 in malignant progression of cancer. Cancer Metastasis Rev 28:151-66.
740 15. Taube JH, Herschkowitz JI, Komurov K, Zhou AY, Gupta S, Yang J, Hartwell K,
741 Onder TT, Gupta PB, Evans KW, Hollier BG, Ram PT, Lander ES, Rosen JM,
742 Weinberg RA, Mani SA. 2010. Core epithelial-to-mesenchymal transition interactome
743 gene-expression signature is associated with claudin-low and metaplastic breast
744 cancer subtypes. Proc Natl Acad Sci U S A 107:15449-54.
745 16. Yang J, Weinberg RA. 2008. Epithelial-mesenchymal transition: at the
746 crossroads of development and tumor metastasis. Dev Cell 14:818-29.
747 17. Bidet A, Laharanne E, Achard S, Migeon M, Moreau C, Lippert E. 2016. Analysis
748 of RUNX1 rearrangements: insights into leukaemogenesis mechanisms. Br J
749 Haematol 175:738-740.
750 18. Brettingham-Moore KH, Taberlay PC, Holloway AF. 2015. Interplay between
751 Transcription Factors and the Epigenome: Insight from the Role of RUNX1 in
752 Leukemia. Front Immunol 6:499.
753 19. Chin DW, Watanabe-Okochi N, Wang CQ, Tergaonkar V, Osato M. 2015. Mouse
754 models for core binding factor leukemia. Leukemia 29:1970-80.
755 20. De Braekeleer E, Douet-Guilbert N, Morel F, Le Bris MJ, Ferec C, De Braekeleer
756 M. 2011. RUNX1 translocations and fusion genes in malignant hemopathies. Future
757 Oncol 7:77-91.

758 21. Dowdy CR, Frederick D, Zaidi SK, Colby JL, Lian JB, van Wijnen AJ, Gerstein
759 RM, Stein JL, Stein GS. 2013. A germline point mutation in Runx1 uncouples its role in
760 definitive hematopoiesis from differentiation. Exp Hematol 41:980-991 e1.
761 22. Dowdy CR, Xie R, Frederick D, Hussain S, Zaidi SK, Vradii D, Javed A, Li X,
762 Jones SN, Lian JB, van Wijnen AJ, Stein JL, Stein GS. 2010. Definitive hematopoiesis
763 requires Runx1 C-terminal-mediated subnuclear targeting and transactivation. Hum
764 Mol Genet 19:1048-57.
765 23. Downing JR, Higuchi M, Lenny N, Yeoh AE. 2000. Alterations of the AML1
766 transcription factor in human leukemia. Semin Cell Dev Biol 11:347-60.
767 24. Durst KL, Hiebert SW. 2004. Role of RUNX family members in transcriptional
768 repression and gene silencing. Oncogene 23:4220-4.
769 25. Friedman AD. 2009. Cell cycle and developmental control of hematopoiesis by
770 Runx1. J Cell Physiol 219:520-4.
771 26. Hart SM, Foroni L. 2002. Core binding factor genes and human leukemia.
772 Haematologica 87:1307-23.
773 27. Lam K, Zhang DE. 2012. RUNX1 and RUNX1-ETO: roles in hematopoiesis and
774 leukemogenesis. Front Biosci (Landmark Ed) 17:1120-39.
775 28. Lichtinger M, Ingram R, Hannah R, Muller D, Clarke D, Assi SA, Lie ALM,
776 Noailles L, Vijayabaskar MS, Wu M, Tenen DG, Westhead DR, Kouskoff V, Lacaud G,
777 Gottgens B, Bonifer C. 2012. RUNX1 reshapes the epigenetic landscape at the onset
778 of haematopoiesis. EMBO J 31:4318-33.

779 29. Lo Coco F, Pisegna S, Diverio D. 1997. The AML1 gene: a transcription factor
780 involved in the pathogenesis of myeloid and lymphoid leukemias. Haematologica
781 82:364-70.
782 30. Sood R, Kamikubo Y, Liu P. 2017. Role of RUNX1 in hematological
783 malignancies. Blood 129:2070-2082.
784 31. Browne G, Dragon JA, Hong D, Messier TL, Gordon JA, Farina NH, Boyd JR,
785 VanOudenhove JJ, Perez AW, Zaidi SK, Stein JL, Stein GS, Lian JB. 2016.
786 MicroRNA-378-mediated suppression of Runx1 alleviates the aggressive phenotype of
787 triple-negative MDA-MB-231 human breast cancer cells. Tumour Biol 37:8825-39.
788 32. Browne G, Taipaleenmaki H, Bishop NM, Madasu SC, Shaw LM, van Wijnen AJ,
789 Stein JL, Stein GS, Lian JB. 2015. Runx1 is associated with breast cancer progression
790 in MMTV-PyMT transgenic mice and its depletion in vitro inhibits migration and
791 invasion. J Cell Physiol 230:2522-32.
792 33. Chimge NO, Frenkel B. 2013. The RUNX family in breast cancer: relationships
793 with estrogen signaling. Oncogene 32:2121-30.
794 34. Chimge NO, Little GH, Baniwal SK, Adisetiyo H, Xie Y, Zhang T, O'Laughlin A,
795 Liu ZY, Ulrich P, Martin A, Mhawech-Fauceglia P, Ellis MJ, Tripathy D, Groshen S,
796 Liang C, Li Z, Schones DE, Frenkel B. 2016. RUNX1 prevents oestrogen-mediated
797 AXIN1 suppression and beta-catenin activation in ER-positive breast cancer. Nat
798 Commun 7:10751.
799 35. Ferrari N, Mohammed ZM, Nixon C, Mason SM, Mallon E, McMillan DC, Morris
800 JS, Cameron ER, Edwards J, Blyth K. 2014. Expression of RUNX1 correlates with
801 poor patient prognosis in triple negative breast cancer. PLoS One 9:e100759.

802 36. Janes KA. 2011. RUNX1 and its understudied role in breast cancer. Cell Cycle
803 10:3461-5.
804 37. Recouvreux MS, Grasso EN, Echeverria PC, Rocha-Viegas L, Castilla LH,
805 Schere-Levy C, Tocci JM, Kordon EC, Rubinstein N. 2016. RUNX1 and FOXP3
806 interplay regulates expression of breast cancer related genes. Oncotarget 7:6552-65.
807 38. Wang L, Brugge JS, Janes KA. 2011. Intersection of FOXO- and RUNX1-
808 mediated gene expression programs in single breast epithelial cells during
809 morphogenesis and tumor progression. Proc Natl Acad Sci U S A 108:E803-12.
810 39. Hong D, Messier TL, Tye CE, Dobson JR, Fritz AJ, Sikora KR, Browne G, Stein
811 JL, Lian JB, Stein GS. 2017. Runx1 stabilizes the mammary epithelial cell phenotype
812 and prevents epithelial to mesenchymal transition. Oncotarget 8:17610-17627.
813 40. Sokol ES, Sanduja S, Jin DX, Miller DH, Mathis RA, Gupta PB. 2015.
814 Perturbation-expression analysis identifies RUNX1 as a regulator of human mammary
815 stem cell differentiation. PLoS Comput Biol 11:e1004161.
816 41. van Bragt MP, Hu X, Xie Y, Li Z. 2014. RUNX1, a transcription factor mutated in
817 breast cancer, controls the fate of ER-positive mammary luminal cells. Elife 3:e03881.
818 42. Festuccia N, Gonzalez I, Owens N, Navarro P. 2017. Mitotic bookmarking in
819 development and stem cells. Development 144:3633-3645.
820 43. John S, Workman JL. 1998. Bookmarking genes for activation in condensed
821 mitotic chromosomes. Bioessays 20:275-9.
822 44. Kadauke S, Blobel GA. 2013. Mitotic bookmarking by transcription factors.
823 Epigenetics Chromatin 6:6.

824 45. Lodhi N, Ji Y, Tulin A. 2016. Mitotic bookmarking: maintaining post-mitotic
825 reprogramming of transcription reactivation. Curr Mol Biol Rep 2:10-16.
826 46. Sarge KD, Park-Sarge OK. 2009. Mitotic bookmarking of formerly active genes:
827 keeping epigenetic memories from fading. Cell Cycle 8:818-23.
828 47. Zaidi SK, Lian JB, van Wijnen A, Stein JL, Stein GS. 2017. Mitotic Gene
829 Bookmarking: An Epigenetic Mechanism for Coordination of Lineage Commitment,
830 Cell Identity and Cell Growth. Adv Exp Med Biol 962:95-102.
831 48. Zaidi SK, Young DW, Montecino MA, Lian JB, van Wijnen AJ, Stein JL, Stein GS.
832 2010. Mitotic bookmarking of genes: a novel dimension to epigenetic control. Nat Rev
833 Genet 11:583-9.
834 49. Zaret KS. 2014. Genome reactivation after the silence in mitosis: recapitulating
835 mechanisms of development? Dev Cell 29:132-4.
836 50. Ali SA, Dobson JR, Lian JB, Stein JL, van Wijnen AJ, Zaidi SK, Stein GS. 2012.
837 A RUNX2-HDAC1 co-repressor complex regulates rRNA gene expression by
838 modulating UBF acetylation. J Cell Sci 125:2732-9.
839 51. Ali SA, Zaidi SK, Dacwag CS, Salma N, Young DW, Shakoori AR, Montecino
840 MA, Lian JB, van Wijnen AJ, Imbalzano AN, Stein GS, Stein JL. 2008. Phenotypic
841 transcription factors epigenetically mediate cell growth control. Proc Natl Acad Sci U S
842 A 105:6632-7.
843 52. Ali SA, Zaidi SK, Dobson JR, Shakoori AR, Lian JB, Stein JL, van Wijnen AJ,
844 Stein GS. 2010. Transcriptional corepressor TLE1 functions with Runx2 in epigenetic
845 repression of ribosomal RNA genes. Proc Natl Acad Sci U S A 107:4165-9.

846 53. Bakshi R, Zaidi SK, Pande S, Hassan MQ, Young DW, Montecino M, Lian JB,
847 van Wijnen AJ, Stein JL, Stein GS. 2008. The leukemogenic t(8;21) fusion protein
848 AML1-ETO controls rRNA genes and associates with nucleolar-organizing regions at
849 mitotic chromosomes. J Cell Sci 121:3981-90.
850 54. Pande S, Ali SA, Dowdy C, Zaidi SK, Ito K, Ito Y, Montecino MA, Lian JB, Stein
851 JL, van Wijnen AJ, Stein GS. 2009. Subnuclear targeting of the Runx3 tumor
852 suppressor and its epigenetic association with mitotic chromosomes. J Cell Physiol
853 218:473-9.
854 55. Young DW, Hassan MQ, Pratap J, Galindo M, Zaidi SK, Lee SH, Yang X, Xie R,
855 Javed A, Underwood JM, Furcinitti P, Imbalzano AN, Penman S, Nickerson JA,
856 Montecino MA, Lian JB, Stein JL, van Wijnen AJ, Stein GS. 2007. Mitotic occupancy
857 and lineage-specific transcriptional control of rRNA genes by Runx2. Nature 445:442-
858 6.
859 56. Young DW, Hassan MQ, Yang XQ, Galindo M, Javed A, Zaidi SK, Furcinitti P,
860 Lapointe D, Montecino M, Lian JB, Stein JL, van Wijnen AJ, Stein GS. 2007. Mitotic
861 retention of gene expression patterns by the cell fate-determining transcription factor
862 Runx2. Proc Natl Acad Sci U S A 104:3189-94.
863 57. Zaidi SK, Young DW, Pockwinse SM, Javed A, Lian JB, Stein JL, van Wijnen AJ,
864 Stein GS. 2003. Mitotic partitioning and selective reorganization of tissue-specific
865 transcription factors in progeny cells. Proc Natl Acad Sci U S A 100:14852-7.
866 58. Pallier C, Scaffidi P, Chopineau-Proust S, Agresti A, Nordmann P, Bianchi ME,
867 Marechal V. 2003. Association of chromatin proteins high mobility group box (HMGB)
868 1 and HMGB2 with mitotic chromosomes. Mol Biol Cell 14:3414-26.

869 59. Arampatzi P, Gialitakis M, Makatounakis T, Papamatheakis J. 2013. Gene-
870 specific factors determine mitotic expression and bookmarking via alternate regulatory
871 elements. Nucleic Acids Res 41:2202-15.
872 60. Blobel GA, Kadauke S, Wang E, Lau AW, Zuber J, Chou MM, Vakoc CR. 2009.
873 A reconfigured pattern of MLL occupancy within mitotic chromatin promotes rapid
874 transcriptional reactivation following mitotic exit. Mol Cell 36:970-83.
875 61. Caravaca JM, Donahue G, Becker JS, He X, Vinson C, Zaret KS. 2013.
876 Bookmarking by specific and nonspecific binding of FoxA1 pioneer factor to mitotic
877 chromosomes. Genes Dev 27:251-60.
878 62. Deluz C, Friman ET, Strebinger D, Benke A, Raccaud M, Callegari A, Leleu M,
879 Manley S, Suter DM. 2016. A role for mitotic bookmarking of SOX2 in pluripotency and
880 differentiation. Genes Dev 30:2538-2550.
881 63. Festuccia N, Dubois A, Vandormael-Pournin S, Gallego Tejeda E, Mouren A,
882 Bessonnard S, Mueller F, Proux C, Cohen-Tannoudji M, Navarro P. 2016. Mitotic
883 binding of Esrrb marks key regulatory regions of the pluripotency network. Nat Cell Biol
884 18:1139-1148.
885 64. Kadauke S, Udugama MI, Pawlicki JM, Achtman JC, Jain DP, Cheng Y,
886 Hardison RC, Blobel GA. 2012. Tissue-specific mitotic bookmarking by hematopoietic
887 transcription factor GATA1. Cell 150:725-37.
888 65. Lake RJ, Tsai PF, Choi I, Won KJ, Fan HY. 2014. RBPJ, the major transcriptional
889 effector of Notch signaling, remains associated with chromatin throughout mitosis,
890 suggesting a role in mitotic bookmarking. PLoS Genet 10:e1004204.

891 66. Lerner J, Bagattin A, Verdeguer F, Makinistoglu MP, Garbay S, Felix T, Heidet L,
892 Pontoglio M. 2016. Human mutations affect the epigenetic/bookmarking function of
893 HNF1B. Nucleic Acids Res 44:8097-111.
894 67. Liu Y, Pelham-Webb B, Di Giammartino DC, Li J, Kim D, Kita K, Saiz N, Garg V,
895 Doane A, Giannakakou P, Hadjantonakis AK, Elemento O, Apostolou E. 2017.
896 Widespread Mitotic Bookmarking by Histone Marks and Transcription Factors in
897 Pluripotent Stem Cells. Cell Rep 19:1283-1293.
898 68. Lodhi N, Kossenkov AV, Tulin AV. 2014. Bookmarking promoters in mitotic
899 chromatin: poly(ADP-ribose)polymerase-1 as an epigenetic mark. Nucleic Acids Res
900 42:7028-38.
901 69. Teves SS, An L, Hansen AS, Xie L, Darzacq X, Tjian R. 2016. A dynamic mode
902 of mitotic bookmarking by transcription factors. Elife 5.
903 70. Xing H, Wilkerson DC, Mayhew CN, Lubert EJ, Skaggs HS, Goodson ML, Hong
904 Y, Park-Sarge OK, Sarge KD. 2005. Mechanism of hsp70i gene bookmarking. Science
905 307:421-3.
906 71. Jordan P, Mannervik M, Tora L, Carmo-Fonseca M. 1996. In vivo evidence that
907 TATA-binding protein/SL1 colocalizes with UBF and RNA polymerase I when rRNA
908 synthesis is either active or inactive. The Journal of Cell Biology 133:225-234.
909 72. Chen CCL, Goyal P, Karimi MM, Abildgaard MH, Kimura H, Lorincz MC. 2018.
910 H3S10ph broadly marks early-replicating domains in interphase ESCs and shows
911 reciprocal antagonism with H3K9me2. Genome Res 28:37-51.
912 73. Goto H, Tomono Y, Ajiro K, Kosako H, Fujita M, Sakurai M, Okawa K, Iwamatsu
913 A, Okigaki T, Takahashi T, Inagaki M. 1999. Identification of a novel phosphorylation

914 site on histone H3 coupled with mitotic chromosome condensation. J Biol Chem
915 274:25543-9.
916 74. Shrivastava T, Mino K, Babayeva ND, Baranovskaya OI, Rizzino A, Tahirov TH.
917 2014. Structural basis of Ets1 activation by Runx1. Leukemia 28:2040-8.
918 75. Gébrane-Younès J, Fomproix N, Hernandez-Verdun D. 1997. When rDNA
919 transcription is arrested during mitosis, UBF is still associated with non-condensed
920 rDNA. Journal of Cell Science 110 (Pt 19):2429-2440.
921 76. Carlton AL, Illendula A, Gao Y, Llaneza DC, Boulton A, Shah A, Rajewski RA,
922 Landen CN, Wotton D, Bushweller JH. 2018. Small molecule inhibition of the
923 CBFbeta/RUNX interaction decreases ovarian cancer growth and migration through
924 alterations in genes related to epithelial-to-mesenchymal transition. Gynecol Oncol
925 149:350-360.
926 77. Illendula A, Gilmour J, Grembecka J, Tirumala VSS, Boulton A, Kuntimaddi A,
927 Schmidt C, Wang L, Pulikkan JA, Zong H, Parlak M, Kuscu C, Pickin A, Zhou Y, Gao
928 Y, Mishra L, Adli M, Castilla LH, Rajewski RA, Janes KA, Guzman ML, Bonifer C,
929 Bushweller JH. 2016. Small Molecule Inhibitor of CBFbeta-RUNX Binding for RUNX
930 Transcription Factor Driven Cancers. EBioMedicine 8:117-131.
931 78. Kim W, Barron DA, San Martin R, Chan KS, Tran LL, Yang F, Ressler SJ,
932 Rowley DR. 2014. RUNX1 is essential for mesenchymal stem cell proliferation and
933 myofibroblast differentiation. Proc Natl Acad Sci U S A 111:16389-94.
934 79. Wu D, Ozaki T, Yoshihara Y, Kubo N, Nakagawara A. 2013. Runt-related
935 transcription factor 1 (RUNX1) stimulates tumor suppressor p53 protein in response to
936 DNA damage through complex formation and acetylation. J Biol Chem 288:1353-64.

937 80. Ozaki T, Nakagawara A, Nagase H. 2013. RUNX Family Participates in the
938 Regulation of p53-Dependent DNA Damage Response. Int J Genomics 2013:271347.
939 81. Satoh Y, Matsumura I, Tanaka H, Harada H, Harada Y, Matsui K, Shibata M,
940 Mizuki M, Kanakura Y. 2012. C-terminal mutation of RUNX1 attenuates the DNA-
941 damage repair response in hematopoietic stem cells. Leukemia 26:303-11.
942 82. Xu L, Gu ZH, Li Y, Zhang JL, Chang CK, Pan CM, Shi JY, Shen Y, Chen B,
943 Wang YY, Jiang L, Lu J, Xu X, Tan JL, Chen Y, Wang SY, Li X, Chen Z, Chen SJ.
944 2014. Genomic landscape of CD34+ hematopoietic cells in myelodysplastic syndrome
945 and gene mutation profiles as prognostic markers. Proc Natl Acad Sci U S A
946 111:8589-94.
947 83. Cargnello M, Tcherkezian J, Roux PP. 2015. The expanding role of mTOR in
948 cancer cell growth and proliferation. Mutagenesis 30:169-76.
949 84. Ciruelos Gil EM. 2014. Targeting the PI3K/AKT/mTOR pathway in estrogen
950 receptor-positive breast cancer. Cancer Treat Rev 40:862-71.
951 85. Feng Y, Manka D, Wagner KU, Khan SA. 2007. Estrogen receptor-alpha
952 expression in the mammary epithelium is required for ductal and alveolar
953 morphogenesis in mice. Proc Natl Acad Sci U S A 104:14718-23.
954 86. Mallepell S, Krust A, Chambon P, Brisken C. 2006. Paracrine signaling through
955 the epithelial estrogen receptor alpha is required for proliferation and morphogenesis
956 in the mammary gland. Proc Natl Acad Sci U S A 103:2196-201.
957 87. Mueller SO, Clark JA, Myers PH, Korach KS. 2002. Mammary gland
958 development in adult mice requires epithelial and stromal estrogen receptor alpha.
959 Endocrinology 143:2357-65.

960 88. Stender JD, Kim K, Charn TH, Komm B, Chang KC, Kraus WL, Benner C, Glass
961 CK, Katzenellenbogen BS. 2010. Genome-wide analysis of estrogen receptor alpha
962 DNA binding and tethering mechanisms identifies Runx1 as a novel tethering factor in
963 receptor-mediated transcriptional activation. Mol Cell Biol 30:3943-55.
964 89. Barutcu AR, Hong D, Lajoie BR, McCord RP, van Wijnen AJ, Lian JB, Stein JL,
965 Dekker J, Imbalzano AN, Stein GS. 2016. RUNX1 contributes to higher-order
966 chromatin organization and gene regulation in breast cancer cells. Biochim Biophys
967 Acta 1859:1389-1397.
968 90. Theodorou V, Stark R, Menon S, Carroll JS. 2013. GATA3 acts upstream of
969 FOXA1 in mediating ESR1 binding by shaping enhancer accessibility. Genome Res
970 23:12-22.
971 91. Gutschner T, Hammerle M, Diederichs S. 2013. MALAT1 -- a paradigm for long
972 noncoding RNA function in cancer. J Mol Med (Berl) 91:791-801.
973 92. Yu X, Li Z, Zheng H, Chan MT, Wu WK. 2017. NEAT1: A novel cancer-related
974 long non-coding RNA. Cell Prolif 50:e12329.
975 93. Li X, Cao Y, Li M, Jin F. 2018. Upregulation of HES1 Promotes Cell Proliferation
976 and Invasion in Breast Cancer as a Prognosis Marker and Therapy Target via the AKT
977 Pathway and EMT Process. J Cancer 9:757-766.
978 94. Strom A, Arai N, Leers J, Gustafsson JA. 2000. The Hairy and Enhancer of Split
979 homologue-1 (HES-1) mediates the proliferative effect of 17beta-estradiol on breast
980 cancer cell lines. Oncogene 19:5951-3.

95. Weyemi U, Redon CE, Sethi TK, Burrell AS, Jailwala P, Kasoji M, Abrams N, Merchant A, Bonner WM. 2016. Twist1 and Slug mediate H2AX-regulated epithelial-mesenchymal transition in breast cells. Cell Cycle 15:2398-404.

96. Kageyama R, Ohtsuka T, Kobayashi T. 2007. The Hes gene family: repressors and oscillators that orchestrate embryogenesis. Development 134:1243-51.

97. Rani A, Greenlaw R, Smith RA, Galustian C. 2016. HES1 in immunity and cancer. Cytokine Growth Factor Rev 30:113-7.

98. Zhang Y, Liu T, Meyer CA, Eeckhoute J, Johnson DS, Bernstein BE, Nusbaum C, Myers RM, Brown M, Li W, Liu XS. 2008. Model-based analysis of ChIP-Seq (MACS). Genome Biol 9:R137.

99. Li QH, Brown JB, Huang HY, Bickel PJ. 2011. Measuring Reproducibility of High-Throughput Experiments. Annals of Applied Statistics 5:1752-1779.

100. Landt SG, Marinov GK, Kundaje A, Kheradpour P, Pauli F, Batzoglou S, Bernstein BE, Bickel P, Brown JB, Cayting P, Chen Y, DeSalvo G, Epstein C, Fisher-Aylor KI, Euskirchen G, Gerstein M, Gertz J, Hartemink AJ, Hoffman MM, Iyer VR, Jung YL, Karmakar S, Kellis M, Kharchenko PV, Li Q, Liu T, Liu XS, Ma L, Milosavljevic A, Myers RM, Park PJ, Pazin MJ, Perry MD, Raha D, Reddy TE, Rozowsky J, Shoresh N, Sidow A, Slattery M, Stamatoyannopoulos JA, Tolstorukov MY, White KP, Xi S, Farnham PJ, Lieb JD, Wold BJ, Snyder M. 2012. ChIP-seq guidelines and practices of the ENCODE and modENCODE consortia. Genome Res 22:1813-31.

101. Dobin A, Davis CA, Schlesinger F, Drenkow J, Zaleski C, Jha S, Batut P, Chaisson M, Gingeras TR. 2013. STAR: ultrafast universal RNA-seq aligner. Bioinformatics 29:15-21.

102. Anders S, Pyl PT, Huber W. 2015. HTSeq--a Python framework to work with high-throughput sequencing data. Bioinformatics 31:166-9.

103. Anders S, Huber W. 2010. Differential expression analysis for sequence count data. Genome Biol 11:R106.

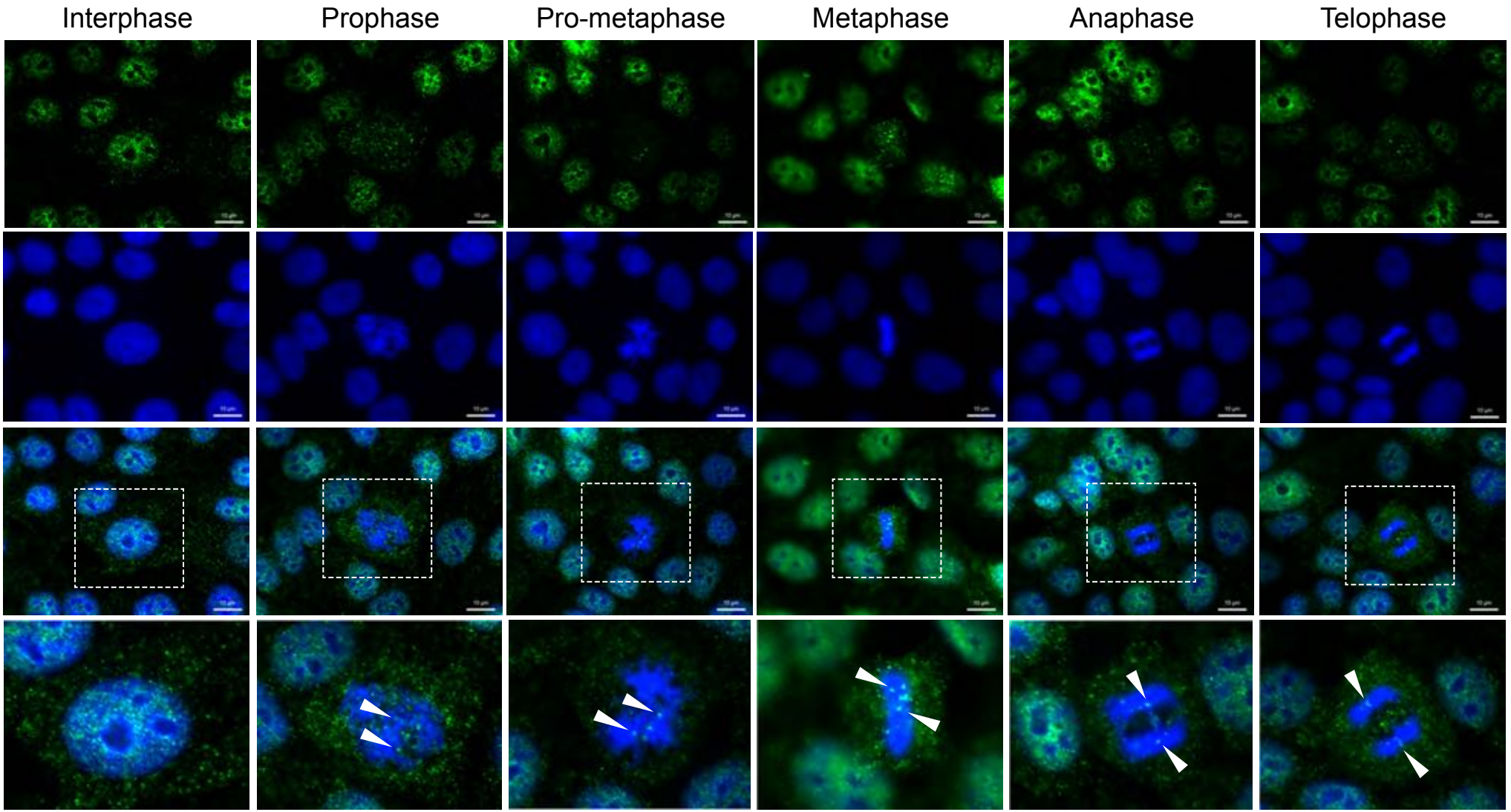
Interphase
Prophase
Pro-metaphase
Metaphase
Anaphase
Telophase
RUNX1
DAPI
MERGED
INSET

Figure 1

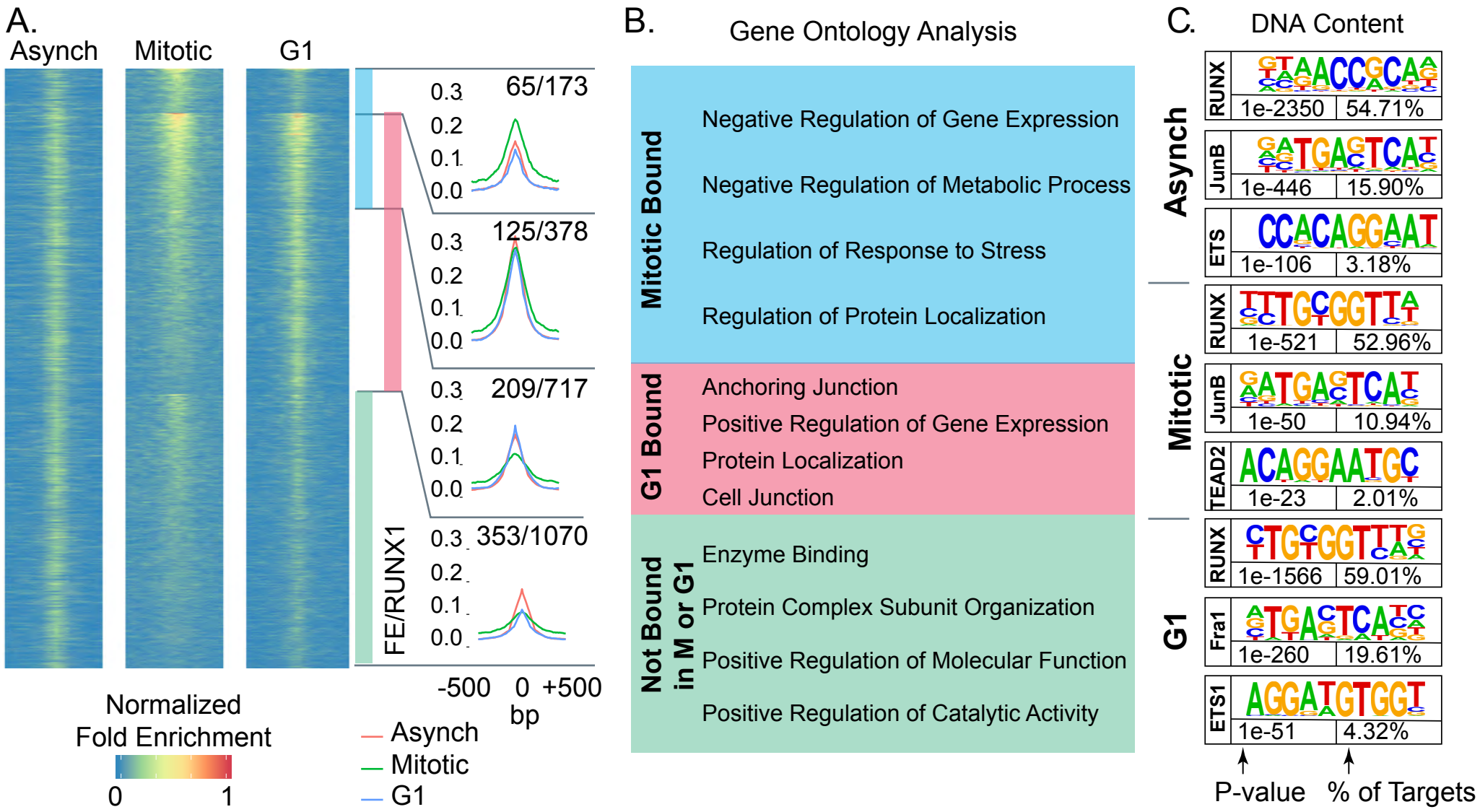
A.
Asynch
Mitotic
G1
65/173
125/378
209/717
353/1070
FE/RUNX1
0.3
0.2
0.1
0.0
-500
0
+500
bp
Normalized
Fold Enrichment
0
1
Asynch
Mitotic
G1
B.
Gene Ontology Analysis
Mitotic Bound
Negative Regulation of Gene Expression
Negative Regulation of Metabolic Process
Regulation of Response to Stress
Regulation of Protein Localization
G1 Bound
Anchoring Junction
Positive Regulation of Gene Expression
Protein Localization
Cell Junction
Not Bound in M or G1
Enzyme Binding
Protein Complex Subunit Organization
Positive Regulation of Molecular Function
Positive Regulation of Catalytic Activity
C.
DNA Content
Asynch
RUNX
1e-2350
54.71%
JunB
1e-446
15.90%
ETS
1e-106
3.18%
Mitotic
RUNX
1e-521
52.96%
JunB
1e-50
10.94%
TEAD2
1e-23
2.01%
G1
RUNX
1e-1566
59.01%
Fra1
1e-260
19.61%
ETS1
1e-51
4.32%
P-value
% of Targets

Figure 2

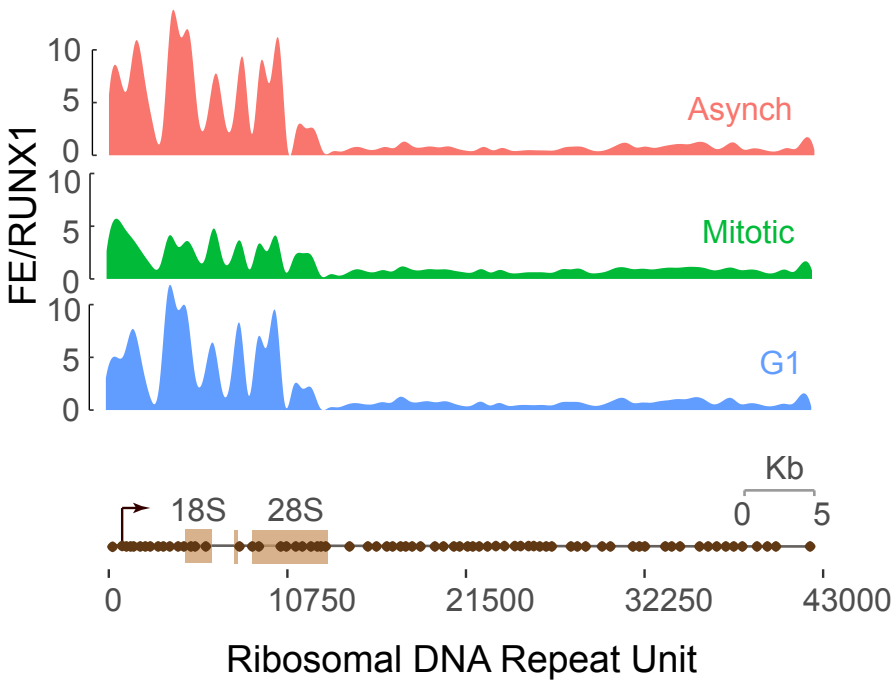
A Genomic Tracks
FE/RUNX1
10
5
0
Asynch
Mitotic
G1
Kb
0
5
18S
28S
0
10750
21500
32250
43000
Ribosomal DNA Repeat Unit

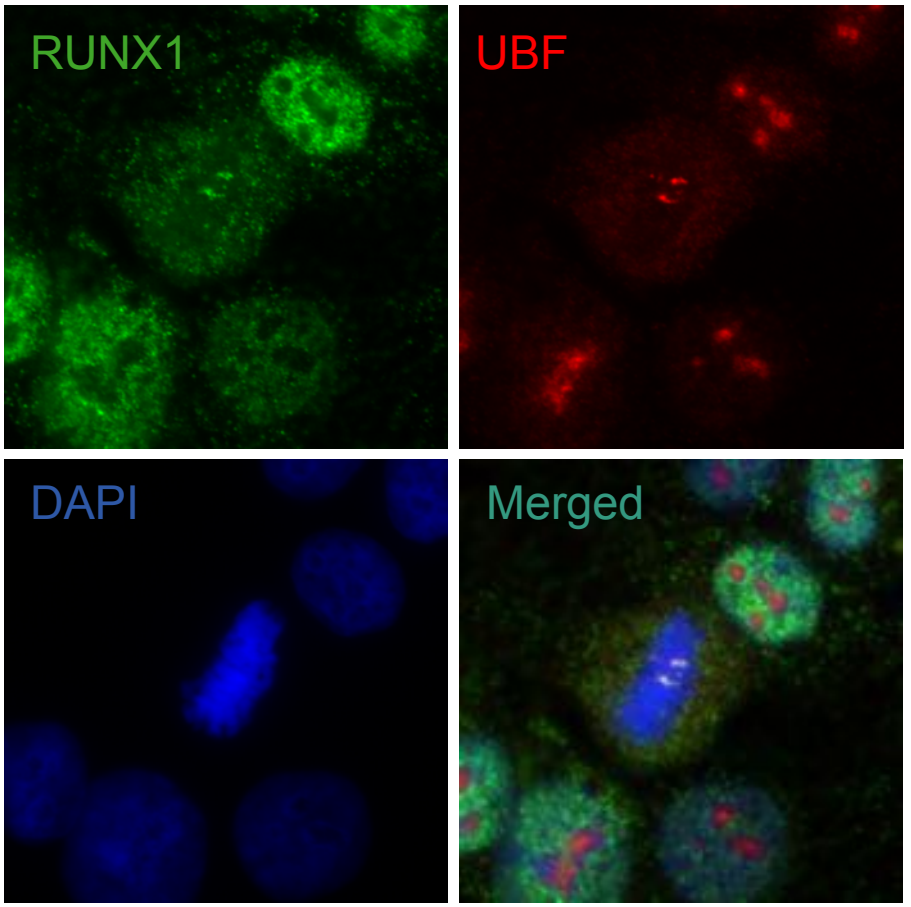
B Immunofluorescence
RUNX1
UBF
DAPI
Merged

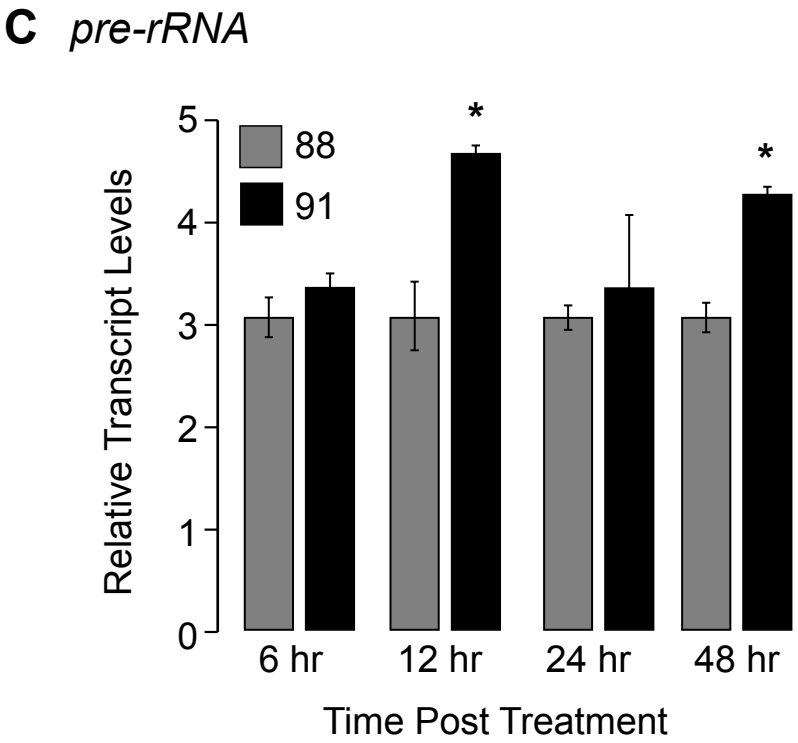
C pre-rRNA
Relative Transcript Levels
88
91
*
*
0
1
2
3
4
5
6 hr
12 hr
24 hr
48 hr
Time Post Treatment

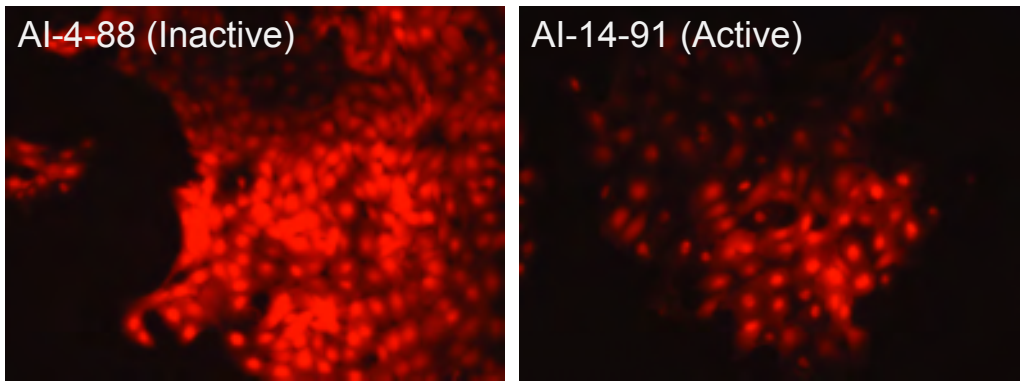
D Protein Label
AI-4-88 (Inactive)
AI-14-91 (Active)

Figure 3

A

Hallmark Gene Set	# of Bookmarked Genes
Late Estrogen Response	12
mTOR Signaling	12
TNFα Signaling	12
Apical Junction	11
Early Estrogen Response	10
G2M Checkpoint	10
p53 Pathway	10
DNA Repair	8
E2F targets	9
Notch Signaling	4

B

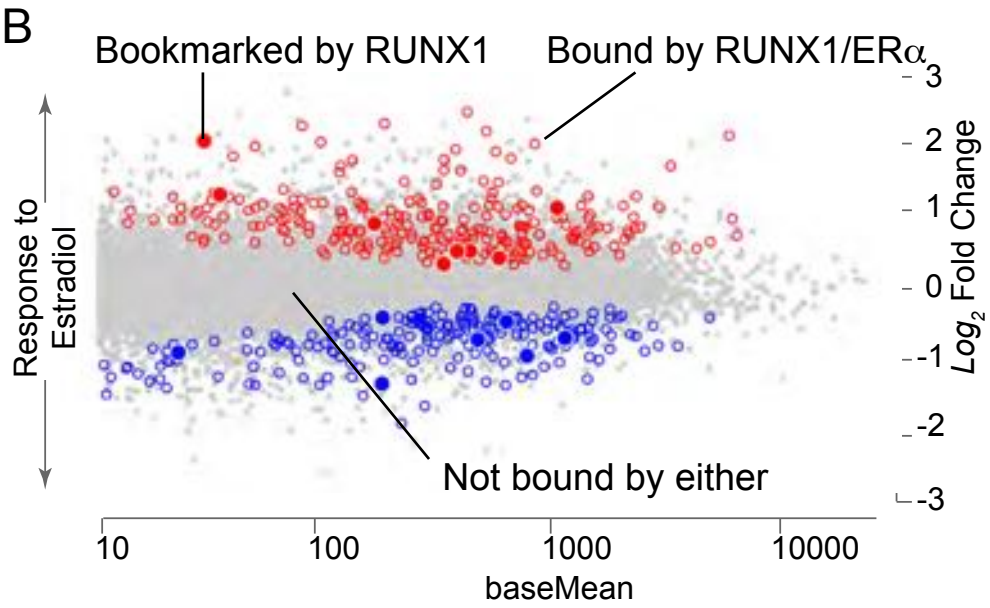

C

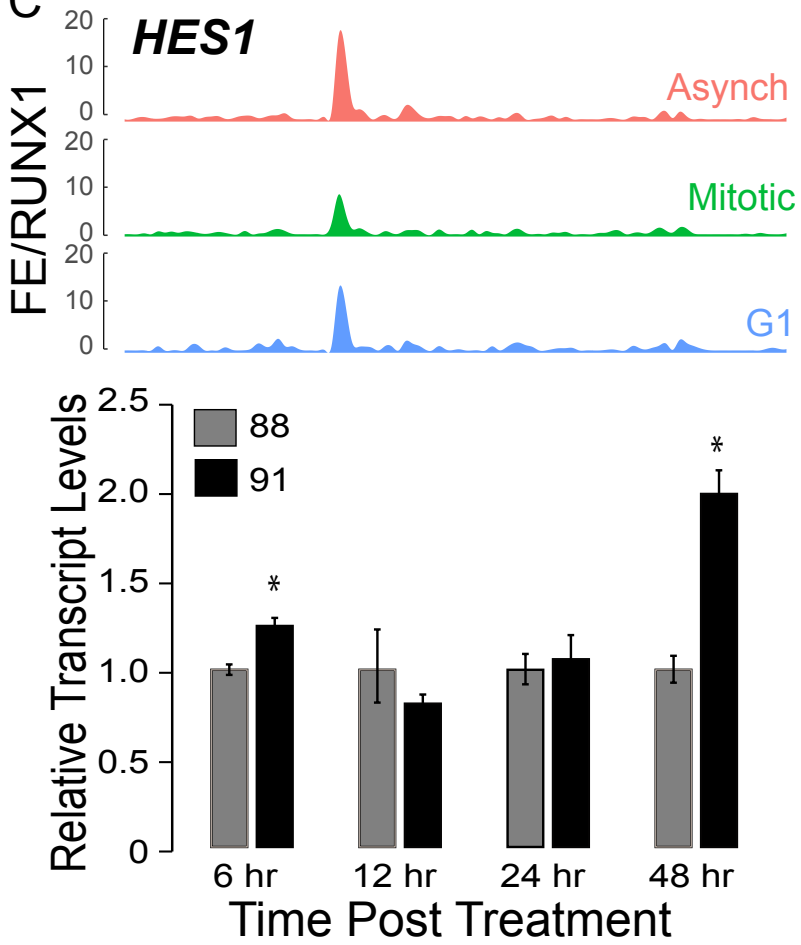

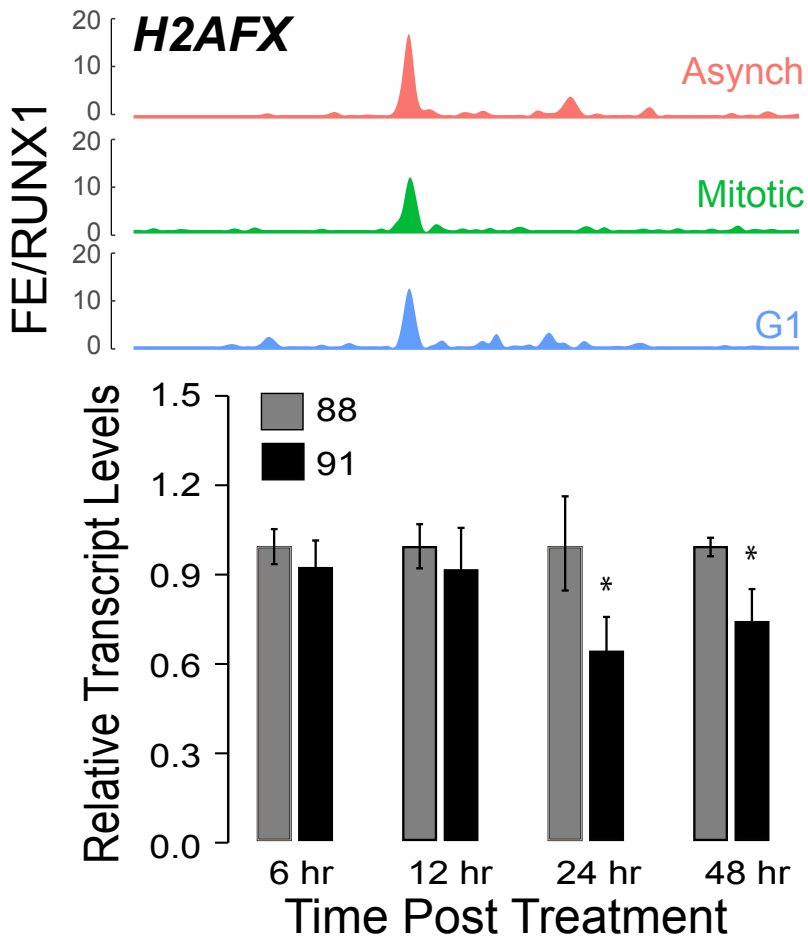

Figure 4

A.

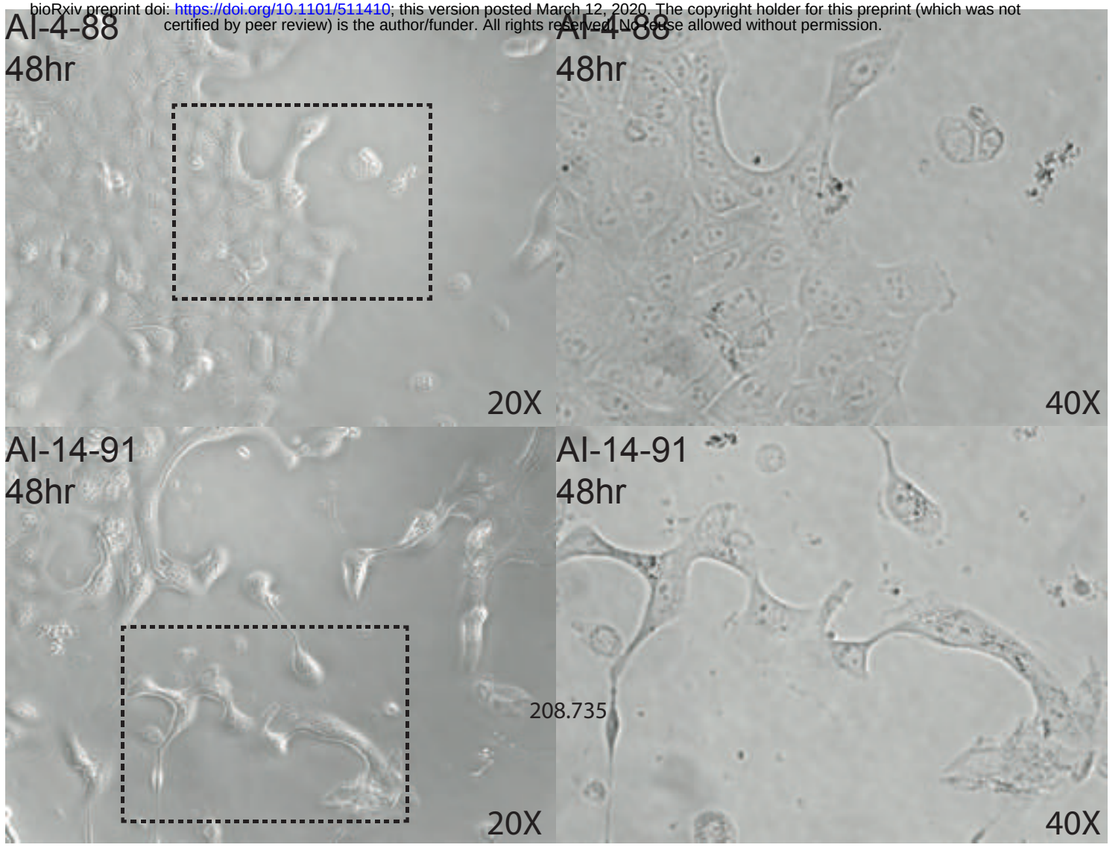

B.

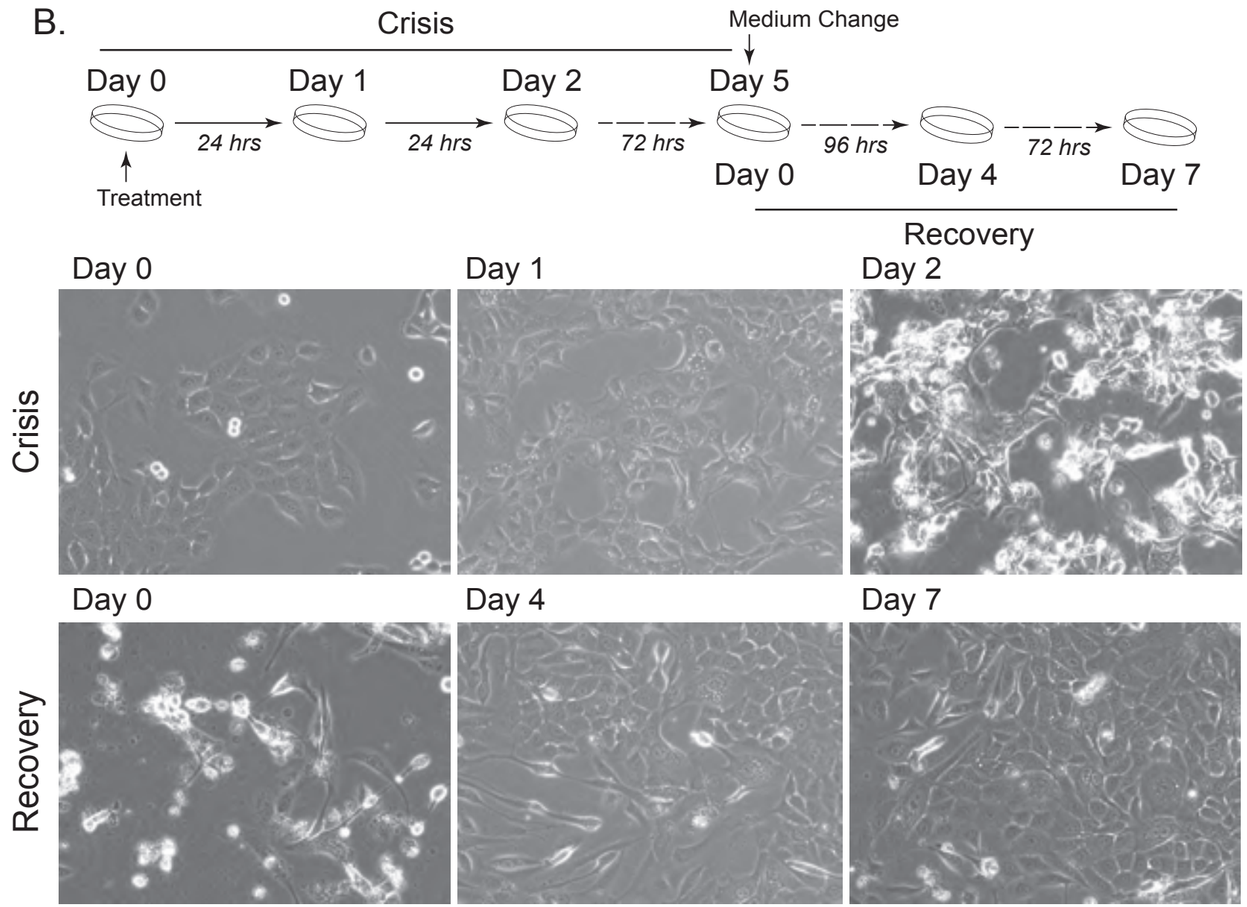

C.

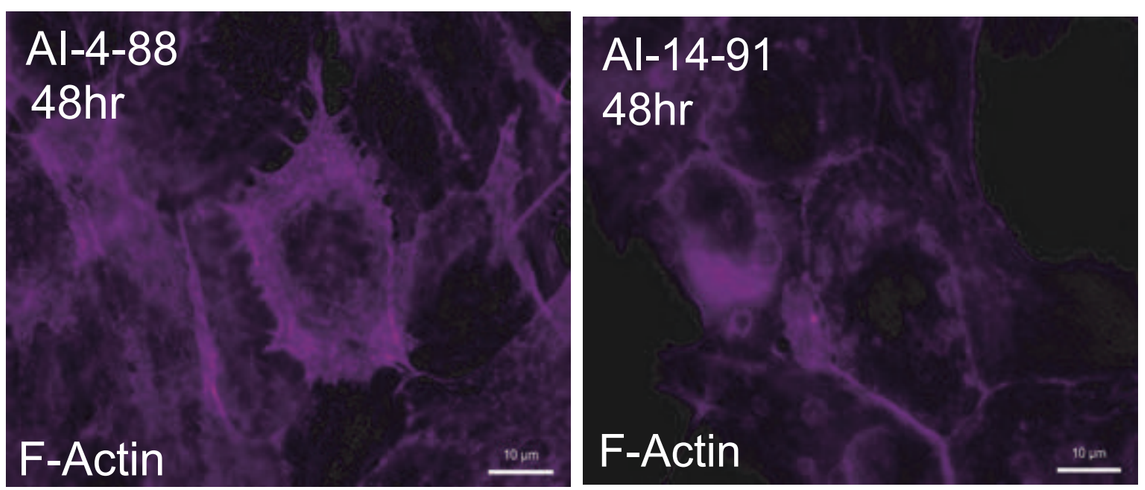

D.

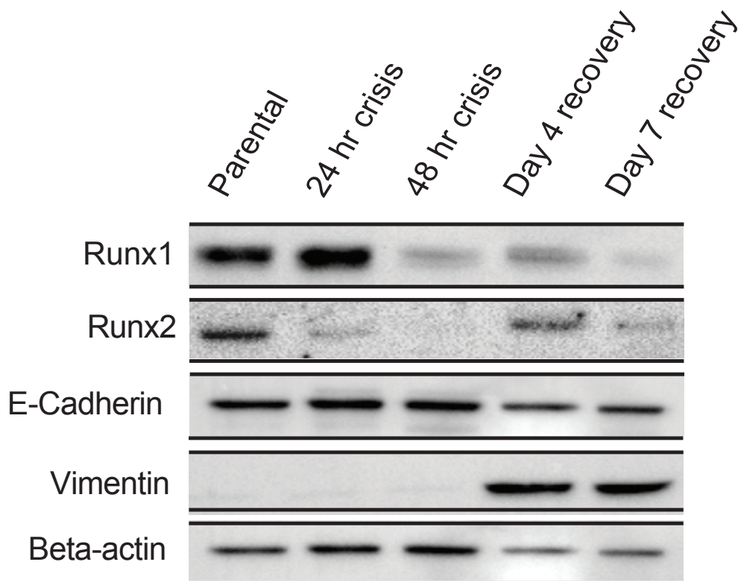

Figure 5

A.

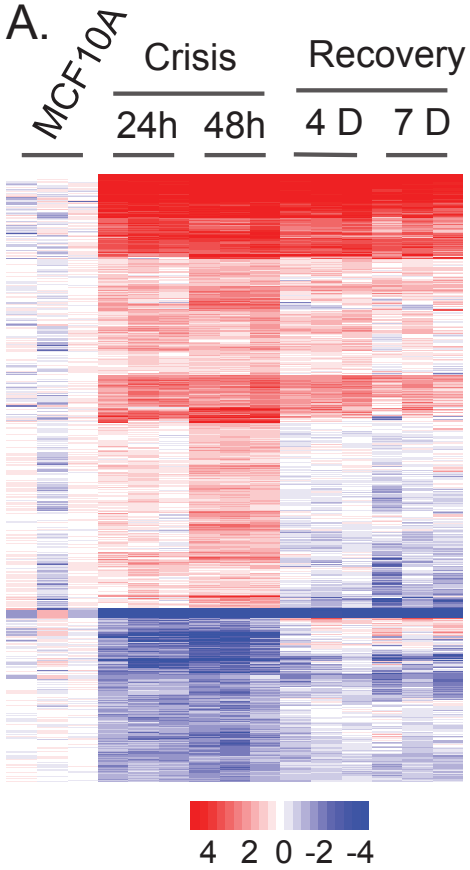

B.

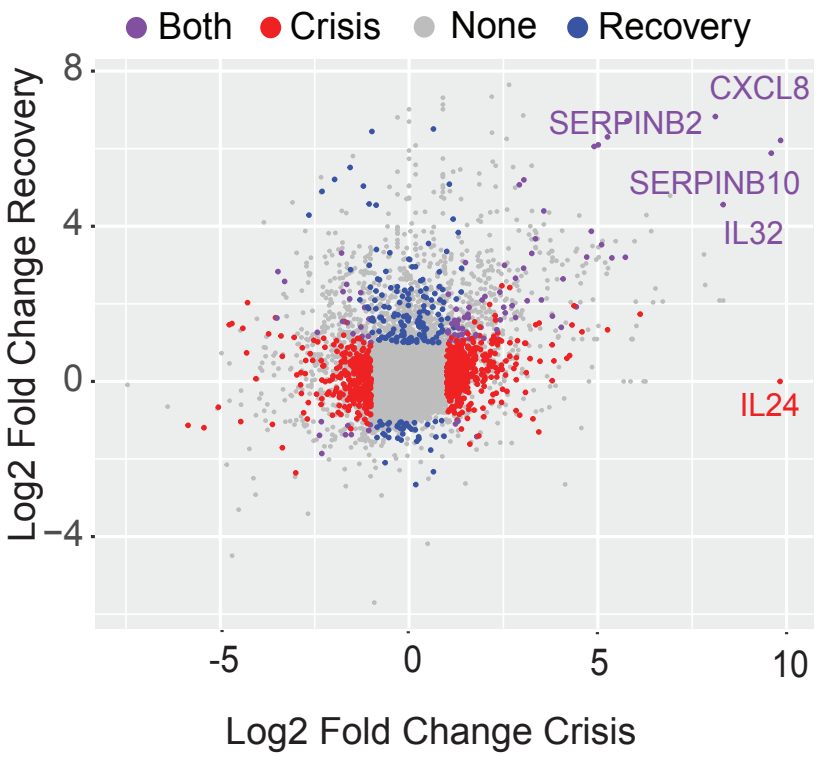

C.

Hallmark Gene Set	Overlapping Crisis DEGs	Enrichment Score
mTORC1 Signaling	35	0.50
TNFα Signaling	69	0.45
Glycolysis	32	0.40
Apoptosis	30	0.26
EMT	28	0.22
p53 Pathway	37	0.20

Hallmark Gene Set	Overlapping Recovery DEGs	Enrichment Score
IFNγ Response	21	0.41
EMT	15	0.40
Complement	19	0.36
TNFα Signaling	27	0.34
KRAS Signaling	22	0.20

D.

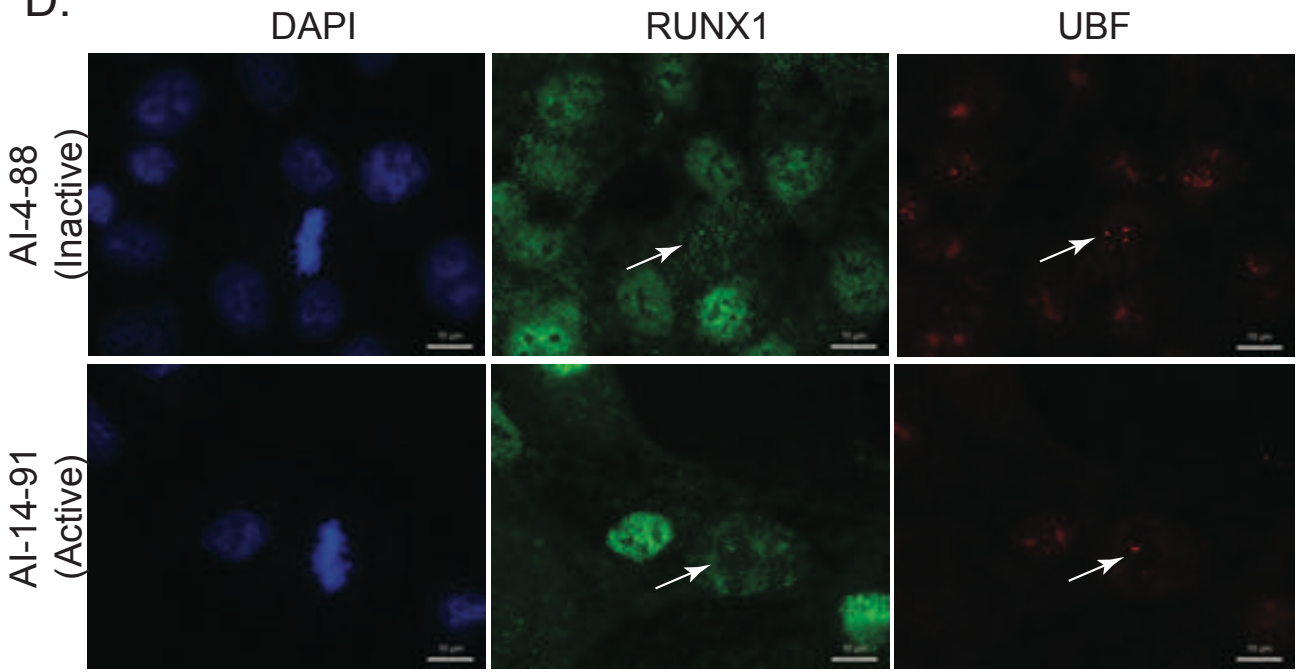

Figure 6

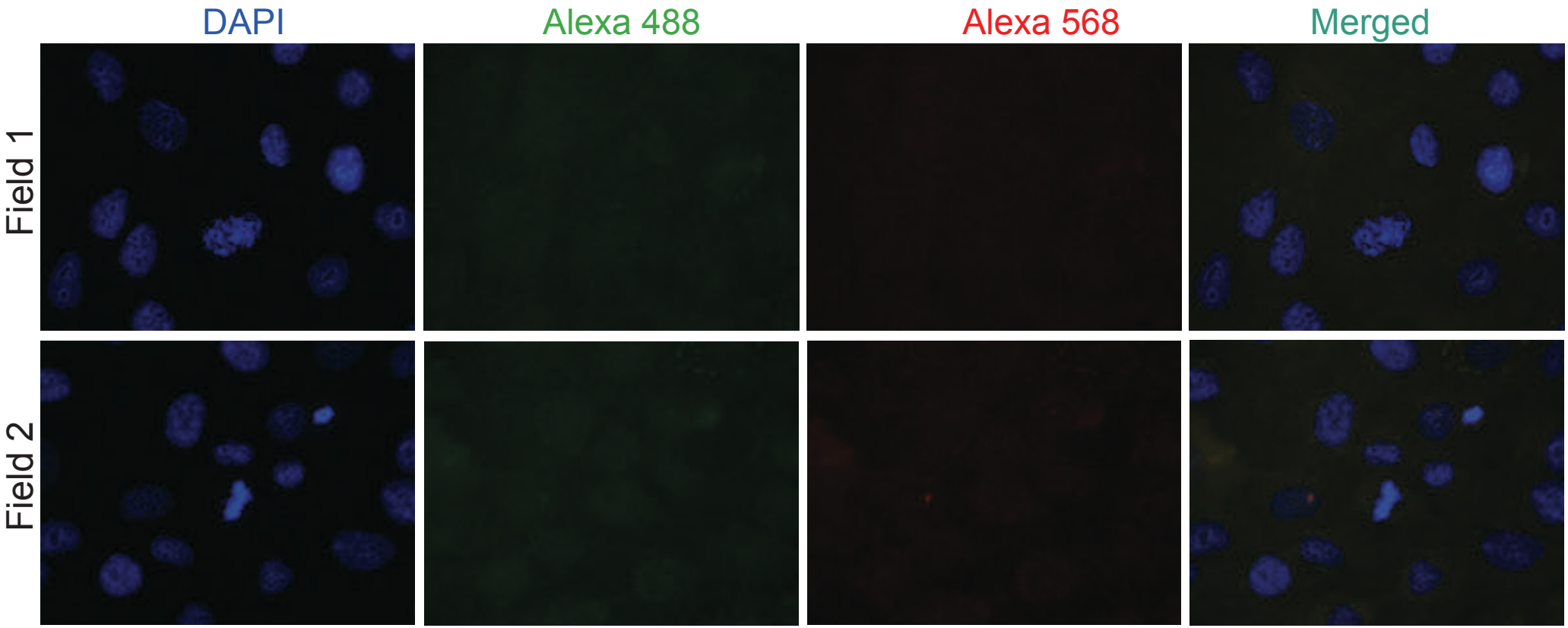

Suppl. Fig. 1

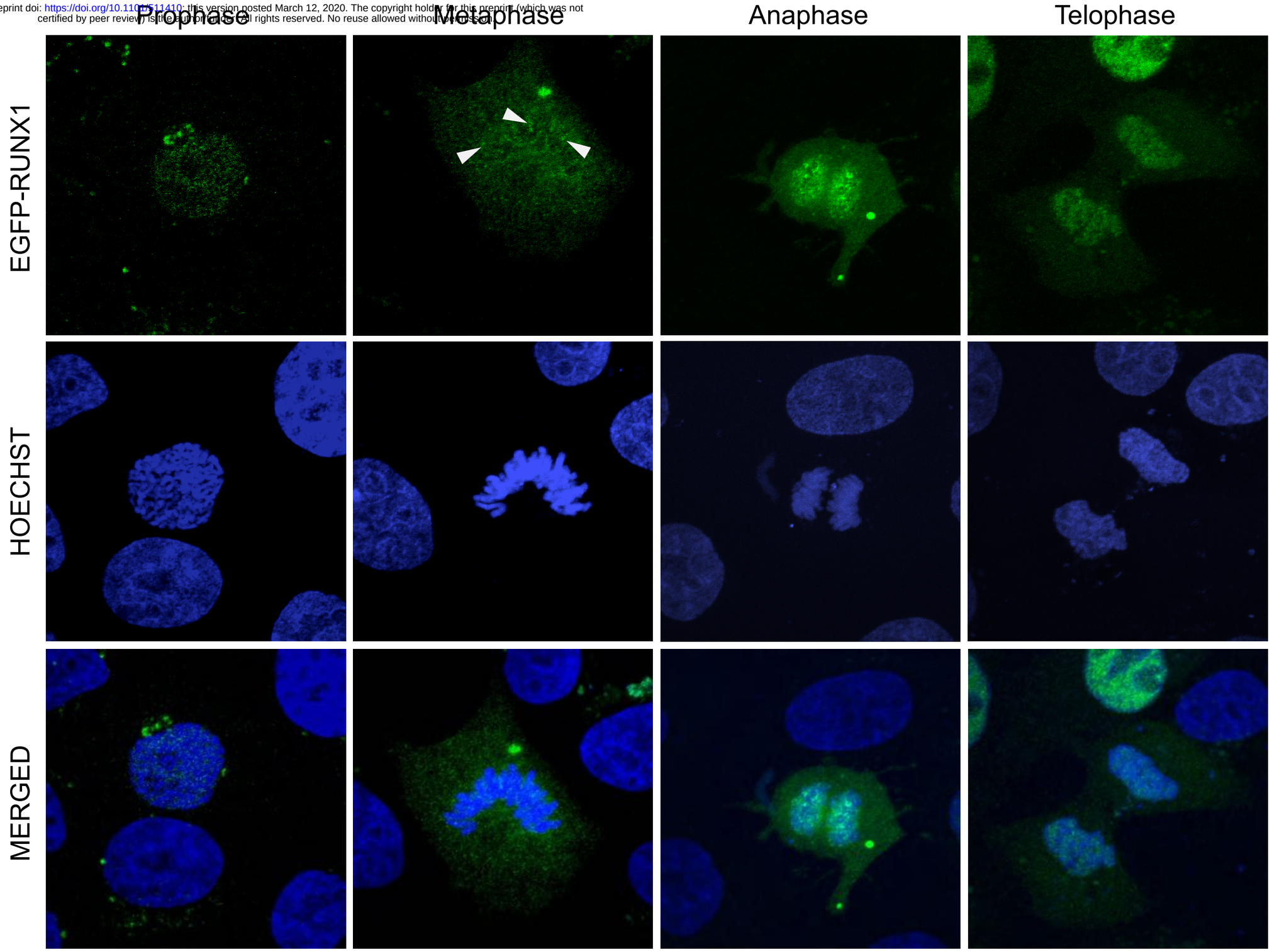

Suppl. Fig. 2

A.

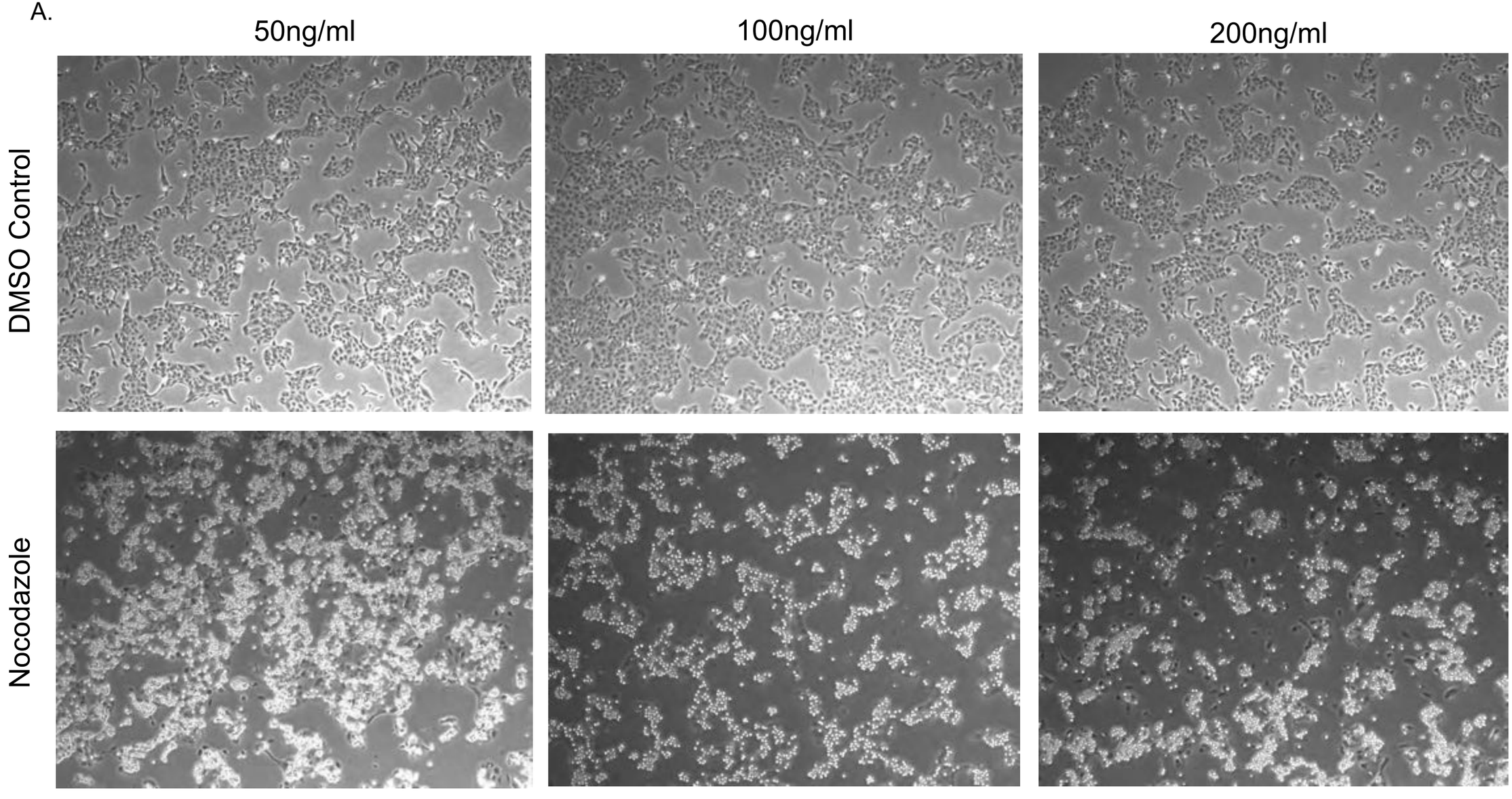

Suppl. Fig. 3

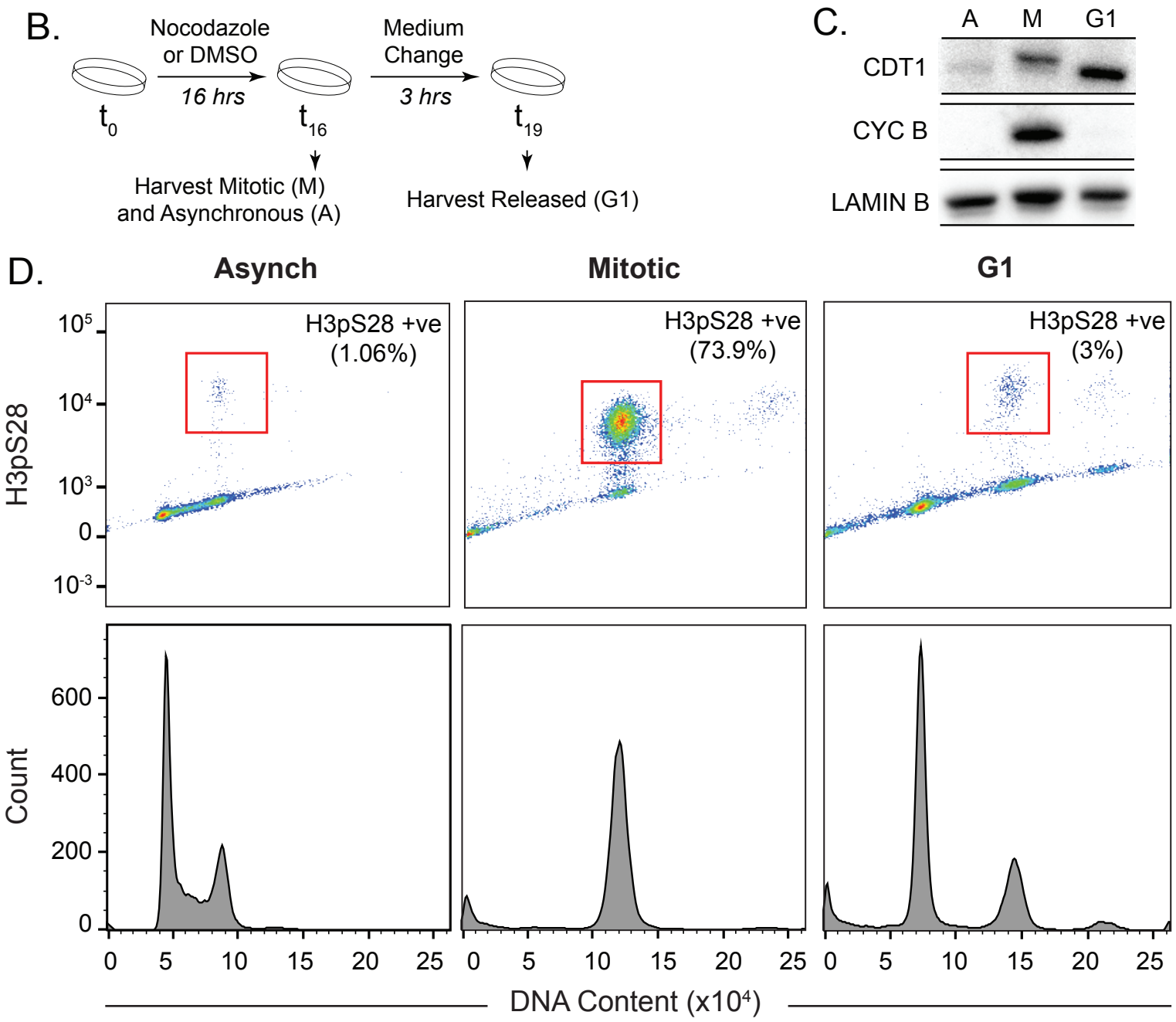
B.
Nocodazole
or DMSO
16 hrs
Medium
Change
3 hrs
t0
t16
t19
Harvest Mitotic (M)
and Asynchronous (A)
Harvest Released (G1)
C.
A
M
G1
CDT1
CYC B
LAMIN B
D.
Asynch
Mitotic
G1
H3pS28 +ve
(1.06%)
H3pS28 +ve
(73.9%)
H3pS28 +ve
(3%)
H3pS28
Count
DNA Content (x10⁴)

Suppl. Fig. 3

A.

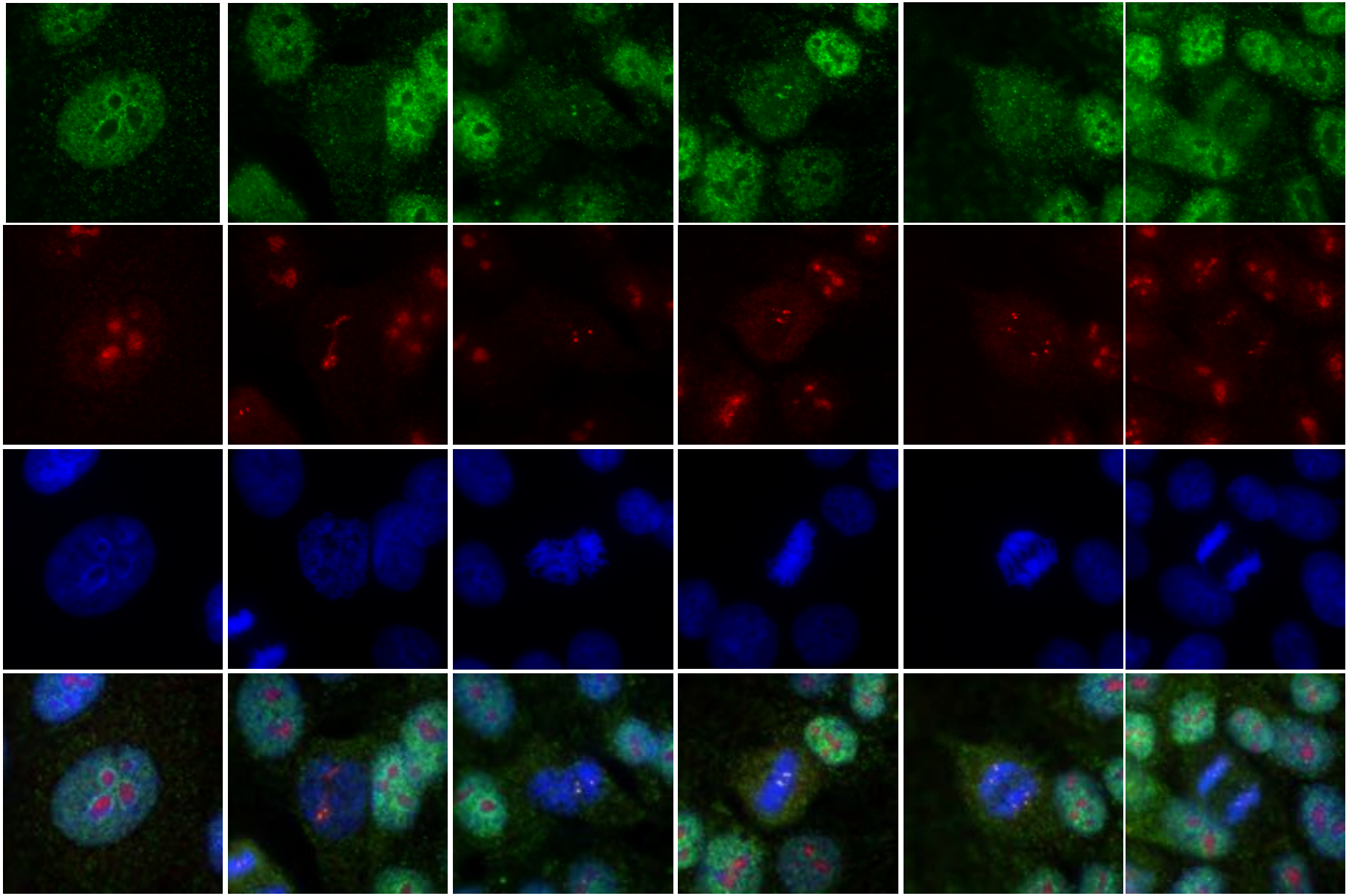

B.

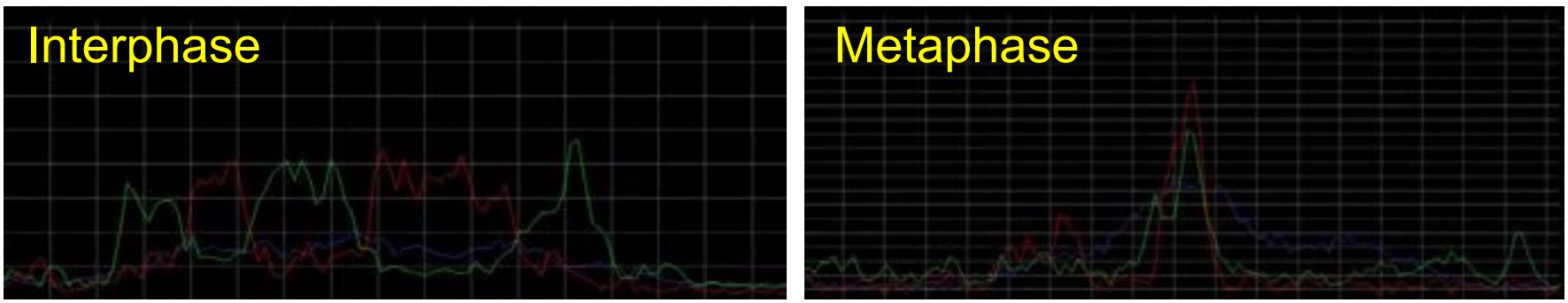

Suppl. Fig. 4

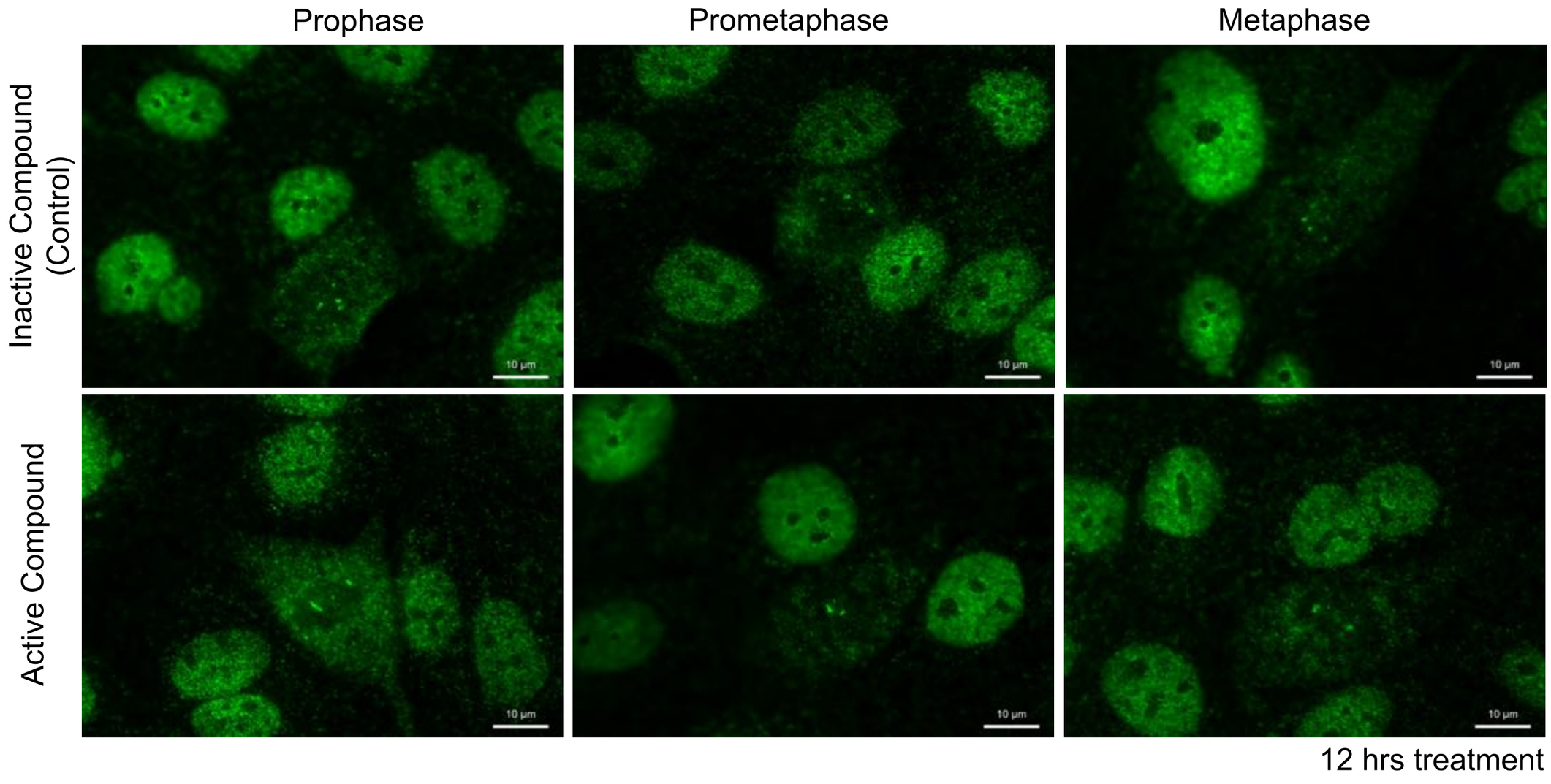

Suppl. Fig. 5